Spring 5-12-2017

GRAPHENE NANORIBBONS AND THEIR POLYMERIC NANOCOMPOSITES: CONTROLLED SYNTHESIS, CHARACTERIZATION AND APPLICATIONS

Nada M. Aljehany
Pittsburg State University, s0o0karh@hotmail.com

Recommended Citation

Aljehany, Nada M., "GRAPHENE NANORIBBONS AND THEIR POLYMERIC NANOCOMPOSITES: CONTROLLED SYNTHESIS, CHARACTERIZATION AND APPLICATIONS" (2017). *Electronic Theses & Dissertations*. 238.
https://digitalcommons.pittstate.edu/etd/238

GRAPHENE NANORIBBONS AND THEIR POLYMERIC NANOCOMPOSITES: CONTROLLED SYNTHESIS, CHARACTERIZATION AND APPLICATIONS

A Thesis Submitted to the Graduate School
In Partial Fulfillment of the Requirements
For The Degree of Master of Science

Nada Aljehany

Pittsburg State University

Pittsburg, Kansas

May, 2017

GRAPHENE NANORIBBONS AND THEIR POLYMERIC NANOCOMPOSITES: CONTROLLED SYNTHESIS, CHARACTERIZATION AND APPLICATIONS

Nada Aljehany

APPROVED:

Thesis Advisor ______________________________
Dr. Ram Gupta, Chemistry Department

Committee Member ______________________________
Dr. Khamis Siam, Chemistry Department

Committee Member ______________________________
Dr. Pawan Kahol, Physics Department

Committee Member ______________________________
Dr. John Franklin, Department of English and Modern Languages

ACKNOWLEDGEMENTS

First of all, I would like to thank my parents and my husband for their support and encouragement. I would like to thank my kids Ajwan, Nayef and Juleen who give me hope and bring me joy; words cannot describe my feeling toward them. I thank them for their great patience at all times.

I would specially like to thank my advisor Dr. Ram Gupta for providing me a great opportunity to perform this research in his group. I truly appreciate him for his guidance and motivation to achieve my goals. I would also like to thank him for teaching me the basics of the chemistry and his patience to improve my skills. Without his guidance, I could not have done this thesis or completed my master's degree.

I would also like to express my sincere thanks to all my committee members, Drs. Khamis Siam, Pawan Kahol and John Franklin and other faculty members in the Chemistry Department at Pittsburg State University. Also, I would like to thank Dr. Sanjay Mishra from University of Memphis, for helping us to record SEM imaging and Raman spectra of our samples.

Last but not least, I would like to thank my lab mates especially John Candler, Charith Ranaweera and Zhuo Wang for their support and help.

GRAPHENE NANORIBBONS AND THEIR POLYMERIC NANOCOMPOSITES: CONTROLLED SYNTHESIS, CHARACTERIZATION AND APPLICATIONS

An Abstract of the Thesis By
Nada Aljehany

Carbon-based materials are very promising as electrode materials energy generation and storage devices. They have been used for fuel cells, supercapacitors and solar cells. Among the carbon-based materials, graphene is very attractive due to its unique properties such as high electrical conductivity, good mechanical flexibility, large theoretical surface area (2630 m^2/g), and high thermal and chemical stability. These unique properties make them very suitable for energy storage applications particularly for supercapacitors. The performance of the graphene as energy storage material could be further improved by growing them in nanoribbon form by unzipping carbon nanotubes. In this thesis, we report synthesis and characterization of graphene nanoribbons from multiwall carbon nanotubes (MWCNT). The synthesized graphene nanoribbons were structurally and electrochemically characterized. The shift of (002) peak in graphene nanoribbons compared to MWCNT confirms unzipping of MWCNT and its exfoliation.

Other materials such as conducting polymers have been also used for energy applications. The performance of the conducting polymers such as polyaniline can be improved by making composites with graphene. We have found that nanocomposites of polyaniline with graphene nanoribbons (PA-GNR) have better performance for energy storage applications. The performance of the nanocomposites, polyaniline and graphene nanoribbons were electrochemically tested using cyclic voltammetry and galvanostatic charge-discharge methods. Cyclic voltammetry was performed at various scan rates to understand the charge transport mechanism. It was observed that the specific capacitance of the PA- GNR nanocomposites decreases with increasing scan rate. The overall charge storage capacity of the PA-GNR composites was higher than that of GNR. The higher charge storage capacity of the PA-GNR composites is due its enhanced surface area and synergistic effect between polyaniline and graphene nanoribbons. A symmetric supercapacitor device was fabricated using PA-GNR composite. The effect of temperature on the charge storage capacity of the device was tested. It was observed that the charge storage capacity of the supercapacitor device increases with an increase in temperature. The results suggest that graphene nanoribbons and composites of polyaniline with graphene nanoribbons could be used as an electrode material for supercapacitor applications.

TABLE OF CONTENTS

CHAPTER PAGE

LIST OF TABLES

TABLE PAGE

LIST OF FIGURES

CHAPTER I

INTRODUCTION

Energy is one of the most important and essentials items to the survival of life. It is very important to explore and develop alternative resources to generate and store the generated energy in a sustainable way. Energy can be generated mainly from two resources; namely, nonrenewable and renewable. Fossil fuels are considered as nonrenewable energy resources and are the main resource for generating energy in developing countries. Energy from solar cells, hydropower and wind are considered as renewable energy. Solar cells, the most popular energy devices, directly convert the solar light into electricity. Hydropower is the other type of renewable energy source. These devices utilize the power of running water to generate energy. Hydropower has several types such as small hydro, micro hydro, conventional hydroelectric, run-of-the-river hydroelectricity and pumped storage hydroelectricity. Wind energy is another important renewable resource to generate energy in a sustainable way. Wind energy is generated using wind turbines or sails. The energy from these natural (and renewable) resources have become very popular; however, most of the generated energy gets wasted due to inefficient energy storage devices. The generated energy needs to be stored efficiently so that we can reduce the energy loss and the energy can be used when needed.

Batteries, fuel cells and capacitors are some of the most popular ways to store energy. A battery stores energy in chemical form and can be converted to electricity when needed. There are two main types of batteries: primary, or non-rechargeable, batteries and secondary batteries, which are rechargeable. Another important energy storage device is capacitors or supercapacitors. Supercapacitors differ from a conventional capacitor in terms of charge storage capacity. Supercapacitors store higher charge (energy) compared to conventional capacitors. Supercapacitors are also known as ultracapacitors or double-layer capacitors (EDLC). A schematic of an EDLC is shown in Figure 1.1.

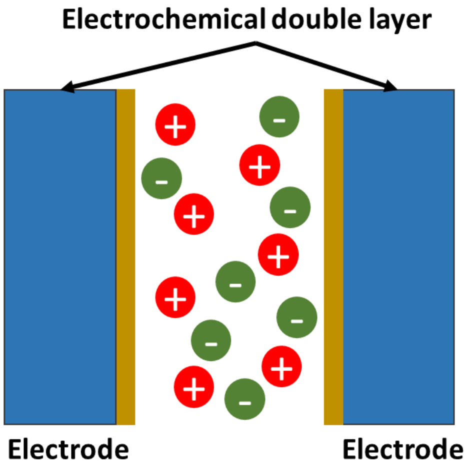

Figure 1.1: Principle of electrical double layer capacitor.

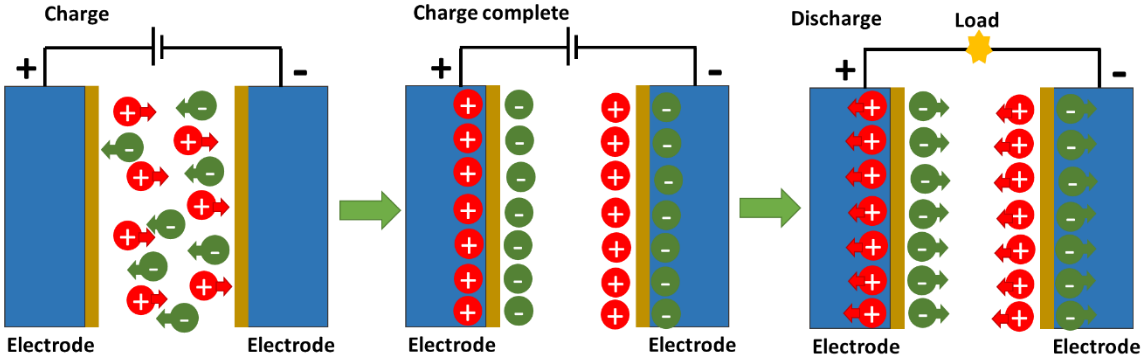

Figure 1.2: EDLS charge-discharge.

In an EDLC, the electric double layer is formed due to separation of the ions. By applying a voltage across the two electrodes, the electrically charged ions in the electrolyte migrate:

positively charged ions move to the negative electrode and negatively charged ions move to the positive electrode, creating two charged layers inside the electrolyte. The charge-discharge process of EDLC is shown in Figure 1.2. The charge-discharge process in conventional capacitor is very fast which provides very high power density. On the other hand, due to the chemical reaction involved, the power density of the batteries is very low, but they provide very high energy density. Supercapacitors are bridging the gap between conventional capacitors and batteries.

Capacitors are mainly classified into three categories based on their charge storage mechanism. The first one is double-layer capacitance (conventional capacitor); the second one is electrochemical pseudocapacitance, where energy is stored due to Faradic reactions. The third one is hybrid capacitors which is a combination of both above mentioned capacitors. In hybrid capacitors, energy is stored due to both electrochemical double-layer and faradic processes. Most of the carbon-based materials store energy due to the formation of electrochemical double layers. Metal oxides and conducting polymers are a few examples of materials used for pseudocapacitors. The classification of the capacitors and most commonly used materials are shown in Figure 1.3. The details of these capacitors are discussed in the following sections.

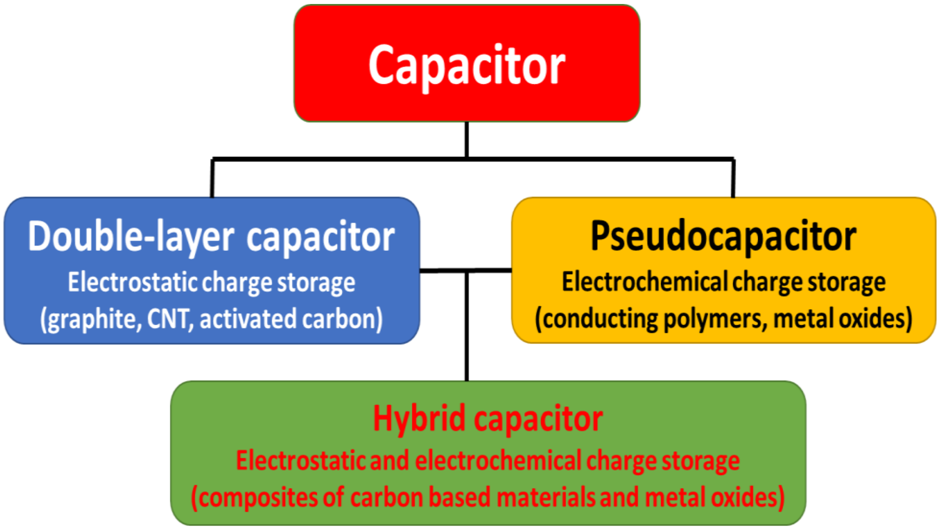

Figure 1.3: Types of Capacitors and materials used.

1.1 Electrical Double-Layer Capacitors (EDLCs)

In EDLCs, the capacitance of the device is directly proportional to the surface area of the electrodes. The materials, such as carbon nanopowders, could provide high specific capacitance due to their large surface area. Commonly in EDLCs, two electrodes made of carbon are used. These electrodes are separated by an ion-transporting layer socked in electrolyte. In EDLCs, there is an accumulation of charges on the surface of the electrode, when the voltage is applied. The ions diffuse across the separator to the pores of the electrode that have an opposite charge. The EDLCs could provide high power densities because of the fast ion transportation [1]. Most commonly, activated carbon is used for the fabrication of EDLCs. Other common materials are graphene (graphite), carbon aerogel, carbide derived carbon, graphene and carbon nanotubes (CNTs).

1.2 Pseudocapacitors

The second most common capacitors are pseudocapacitors. Pseudocapacitors provide higher charge storage capacity compare to EDLCs. The higher charge storage capacity is due to the Faradic reaction involved in the process. Pseudocapacitors store energy due to charge transfer that occurs at the surface of the faradic electrodes. The processes that are involved in charge transfer are reduction-oxidation reactions, electrosorption and the process of intercalation [2-4]. Conducting polymers and metal oxides are the common examples of the materials used for pseudocapacitors.

1.3 Hybrid capacitors

This is the third type of supercapacitors. Hybrid capacitors utilize both mechanisms (electrochemical double layer and Faradic process) to store energy. This type of capacitor provides high energy densities and high power densities compared with electrolyte double-layer capacitors and pseudocapacitors. There are three types of hybrid capacitors that have been executed by their electrode configuration. These are composite, asymmetric, and battery-type [5].

In composite electrodes, carbon-based materials are combined with either metal oxide materials, conducting polymer, or both in one single electrode. This carbon-based material enables a capacitive double-layer of charge storage and they also provide a high-surface-area which can increase the contact between the pseudocapacitive materials (metal oxide materials or conducting polymer) and the electrolyte. The pseudocapacitive materials are themselves able to increase the capacitance of the composite electrode through Faradaic reactions [6]. Composite electrodes made from carbon nanotubes and conducting polymers such as polyaniline have been widely studied. These studies demonstrated that such an electrode is able to deliver higher capacitances compared to pure carbon-based - or pure polyaniline-based electrodes.

Another type of hybrid capacitor is asymmetric hybrids. Asymmetric hybrids combine Faradic and non-Faradic processes by coupling a pseudocapacitor electrode with an electrolyte double-layer electrode. Recently the coupling of a negative carbon electrode with the positive conducting polymer electrode has achieved a greater demand [6]. These types of hybrid capacitors are less stable but could provide higher capacitance. They also show less resistance and high power/energy densities [7].

The third type is battery-type hybrid capacitors. These also couple two different types of electrodes together, like asymmetric hybrid capacitors; however, these are unique as they couple a supercapacitor electrode with a battery electrode. This type of configuration enhances the efficiency of the devices. They have higher energy densities than supercapacitors and also have higher power densities than that of batteries. The electrodes that are mostly used are nickel hydroxide, lead dioxide for one electrode and another electrode is made of activate carbon. This type of capacitor is bridging the gap between batteries and supercapacitors [8,9].

Newly developed supercapacitors are environmentally friendly and could provide high energy [10] . There are many advantages of supercapacitors over batteries. Supercapacitors have longer life and are very safe compared with lithium ion batteries and acid batteries [11]. Supercapacitors are widely used in remote controls, toys, traffics signals etc.[12]. In the following sections, we will focus on some of the materials commonly used for energy storage applications.

1.4 Carbon Nanotubes (CNTs)

Carbon nanotubes are being used as electrode material for energy storage applications, particularly for EDLCs [13]. Such types of capacitors that have CNTs have open and approachable network of mesoporous. In these capacitors, there is a connection between the mesoporous, and they are interlinked. This permits the equal and continuous distribution of charges. Thus, these are more efficient than those of carbon activated and carbon aerogels [14]. These also have low electrical series resistance (ESR) and can even reduce ESR more as compared to activated carbons. Due to this type of network, they have higher energy densities and higher power densities [15]. For example, Wenelska et al. have decorated carbon nanotubes by mesoporous cobalt oxide as an electrode material for lithium-ion batteries [16].

1.5 Graphene

Graphene has a unique structure and distinguished characteristics. It has high electrical conductivity and large surface area. It also has very high mechanical strength. Due to these unique properties, graphene is very suitable for energy applications particularly for solar cell, batteries and supercapacitors [17,18]. Our group has used graphene for supercapacitor applications [19]. It has been observed that graphene-decorated $NiCo_2O_4$ showed better charge storage properties compare with $NiCo_2O_4$. Lai et al. have studied the effect of surface functionalization of graphene on energy storage capacity [20].

1.6 Composites

The main advantages of conducting polymers are their high conductivity and capacitance and low cost in contrast to carbon-based electrode materials such as CNT and graphene [6]. However, they possess low mechanical strengths and stability [21]. Composite electrodes incorporate carbon-based materials with other high energy storage materials such as metal oxides. The carbon-based materials provide high surface area, whereas metal oxides provide high energy storage capacity due to Faradic reaction. This combination provides a material with high energy storage capacity and improved stability [22,23]. The composites of graphene and polyaniline have been synthesized for improved energy storage capacity [24]. The composite electrode showed better energy storage capacity compared with that of individual materials and also showed good cycling stability. The composite materials could be synthesized via various methods such as chemical, interfacial, electrochemical deposition on preformed carbon nanotube electrodes, or by electrochemical co-deposition.

In this work, we have synthesized nanocomposites of graphene nanoribbons with polyaniline. Graphene nanoribbons were synthesized by unzipping carbon nanotubes. The unzipped carbon nanotubes were dispersed in aqueous media using the sonication process and then polyaniline was chemically polymerized over these nanoribbons. The detailed structural and electrochemical characterizations for their applications as electrode materials for supercapacitor were performed.

CHAPTER II

EXPERIMENTAL DETAILS

2.1 Materials and synthesis

The details of the materials used, and synthesis processes of graphene nanoribbon, polyaniline and their composites, are given below:

2.1.1. Synthesis of graphene nanoribbons (GNR)

Graphene nanoribbons were synthesized using multiwall carbon nanotubes with outer diameters of 110-170 nm. In a typical synthesis, 1 g of multiwall carbon nanotubes was dispersed in 280 ml of sulfuric acid (H_2SO_4) and 32 ml of phosphoric acids (H_3PO_4) using magnetic stirrer. To this mixture, 10 g potassium permanganate ($KMnO_4$) was slowly added with constant stirring at 65^{o}C. The mixture was left in this condition for an additional 4 hours. Finally, the reaction mixture was cooled to room temperature and poured over 800 ml of ice water containing hydrogen peroxide (40 ml, 30 %). The resulting mixture was congealed overnight then filtered (using 0.2 µm mesh PTFE from Millipore) and washed in succession with hydrochloric acid (30 %), ethanol (100 %), and diethyl ether (anhydrous). The final black material was dried at 65^{o}C in a vacuum oven for 10 hours.

2.1.2. Synthesis of polyaniline

Polyaniline was chemically polymerized using aniline and ammonium persulfate (APS) in acidic condition. For the synthesis of polyaniline, 0.19 ml of aniline was dissolved in 100 ml of 1M sulfuric acid and then cooled to 5°C using an ice bath. In another beaker, 4.56 g of ammonium per sulfate was dissolved in 50 ml of 1M sulfuric acid, and this solution was also cooled to 5°C. The ammonium persulfate solution was added dropwise to the aniline solution under stirring. Black precipitate started appearing upon the addition of ammonium per sulfate. The mixture was stirred continuously at 5°C for an additional 3 hours. After this, the resulting precipitate was filtered and washed with DI water several times. The obtained powder was dried in vacuum at 50°C for 10 hours.

2.1.3. Synthesis of composites of GNR-polyaniline

The procedure to synthesize composites of GNR-polyaniline was very similar to that of polyaniline. However, different amounts of graphene nanoribbons (Table 2.1) were dispersed in the aniline solution before adding ammonium per sulfate.

Table 2.1: Experimental details for the synthesis of composites of GNR-polyaniline

Sample code	**Aniline in 100 ml 1M H_2SO_4 (ml)**	**APS in 100 ml 1M H_2SO_4 (g)**	**GNR (mg)**
PANI-GNR-105	0.19	4.56	4.65 (0.5 wt %)
PANI-GNR-106	0.19	4.56	9.30 (1 wt %)
PANI-GNR-107	0.19	4.56	23.25 (2.5 wt %)
PANI-GNR-108	0.19	4.56	46.5 (5 wt %)
PANI-GNR-109	0.19	4.56	93.0 (10 wt %)

2.2. Materials characterizations

The synthesized materials were characterized using different techniques such as Fourier transform infrared spectroscopy (FT-IR), X-Ray diffraction (XRD), Raman spectroscopy, scanning electron microscopy (SEM) and electrochemical methods. The details of these techniques are given below:

2.2.1. Fourier transform infrared spectroscopy

Fourier transform infrared spectroscopy (FT-IR) is an analytical technique in which infrared light is used to measure the absorption and emission of liquid, solid or gas, to characterize their properties. The information about the chemical bonds and molecular structure of the material is provided by creating an absorbance spectra of the sample as a function of wavenumber during the FTIR analysis. The FT-IR spectra of all the samples were recorded on a Shimadzu IR Affinity-1. A picture of the FT-IR instrument used is given in Figure 2.1.

Figure 2.1. Picture of FT-IR instrument used.

2.2.2. X-Ray Diffraction

X-ray diffraction (XRD) is a rapid analytical technique that can give information on unit cell dimensions and is used for phase identification of a crystalline material. By using a Shimadzu X-ray diffractometer set in 2θ-θ scan (with CuK$_{\alpha 1}$ radiation, λ=1.5406 Å), the structure of the synthesized materials was investigated. Slits of 0.2 mm were used for the source and detector sides. To generate the X-ray, a voltage of 40 kV and a current of 30 mA were used. By using a detector, diffraction patterns in the form of X-ray counts were collected when the sample was rotated through 2θ = 25° - 70°. A picture of the XRD instrument used is given in Figure 2.2.

Figure 2.2: Picture of XRD instrument used.

2.2.3. Raman spectroscopy

Raman spectroscopy is a spectroscopic technique that is based on inelastic collision of monochromatic light (in most cases it is LASER) with matter; that interaction causes changes in frequency and energy of the incident photons. The photons are absorbed by the sample and are re-emitted; the frequency of re-emitted photons shifts down or up, and this shifting of frequency of the photons is known as the Raman Effect. This provides information about rotational, vibrational and other low frequency transitions taking place in molecules. All types of samples (solid, liquid and gases) can be analyzed by Raman Spectroscopy. When electromagnetic radiation interacts with the molecules, the polarizable electron-cloud density and the bonds in the molecules face change in their environment; this inelastic scattering of the photons either excites the molecules from lower rotational and vibrational energy states to higher rotational and vibrational energy states or de-excites the molecules from higher rotational and vibrational energy states to lower rotational and vibrational energy states. In the results of these excitations and de-excitations, the frequency of incident photons is changed, which is called Raman Shift. A picture of Raman spectroscopy instrument used is given in Figure 2.3.

Figure 2.3: Picture of Raman instrument used.

2.2.4. Scanning electron microscopy characterization

Scanning electron microscopy (SEM) was used to examine the morphologies of the synthesized graphene nanoribbons, polyaniline and their nanocomposites. A JEOL JSM-840A scanning electron microscope and an FEI Quanta 200 field emission scanning electron microscopy (FESEM) equipped with an Oxford INCA 250 silicon drift X-ray energy dispersive spectrometer (EDS) were used to study the particle size and morphology of the powder samples. A picture of the Raman spectroscopy instrument used is given in Figure 2.4.

Figure 2.4: Picture of SEM instrument used.

2.2.5. Electrochemical measurements

The electrochemical measurements were done on a Versastat 4-500 electrochemical workstation (Princeton Applied Research, USA), as shown in Figure 2.5. The electrochemical measurements were performed using the three-electrode system, which consists of a saturated calomel electrode as a reference electrode, a platinum wire as a counter electrode and a working electrode synthesized (GNRs, PANI and PA-GNRs nanocomposites) on nickel foam. The schematic diagram of the three-electrode system is shown in Figure 2.6. Before preparing the working electrode, the nickel foam was cleaned using 3M HCl followed by cleanings using water and acetone respectively with the assistance of ultrasonication. The working electrode was prepared by mixing 80 wt.% of the samples, 10 wt.% of carbon black and 10 wt.% of polyvinylidene difluoride (PVdF) in the presence of N-methyl pyrrolidinone (NMP) that was used as a solvent to make paste. After mixing the components, the nickel foam was dipped in this paste followed by drying at 60°C under vacuum overnight. For all the measurements, 3M KOH was used as electrolyte. Besides electrochemical investigation on single electrode, a symmetric supercapacitor was fabricated and tested as well. The supercapacitor device was assembled by pressing two PA-GNR electrodes together with an ion-transporting layer (Celgard 25 µm, thick, 39% porosity) between as the separator (Figure 2.7). In all experiments performed, 3 M KOH was used as an electrolyte for this assembly. The charge storage capacity of the electrode and device was measured using cyclic voltammetry (CV) and galvanostatic charge-discharge measurements. The study of the effect of temperature on the electrochemical properties of the device was done for its application in rough conditions.

Figure 2.5: Potentiostat used for electrochemical measurements.

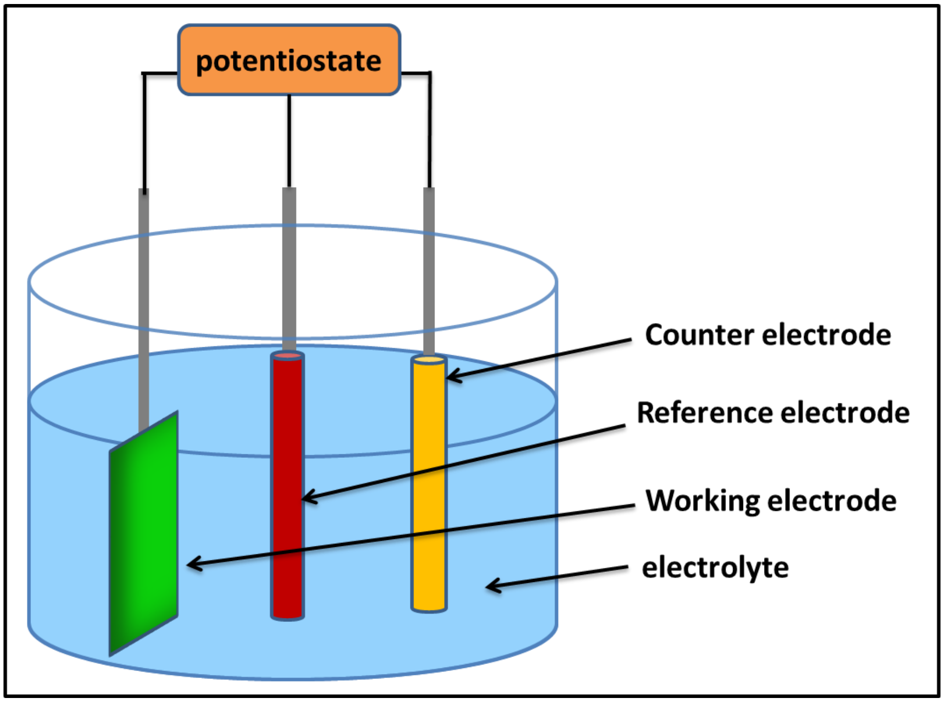

Figure 2.6: The schematic diagram of the three electrodes system.

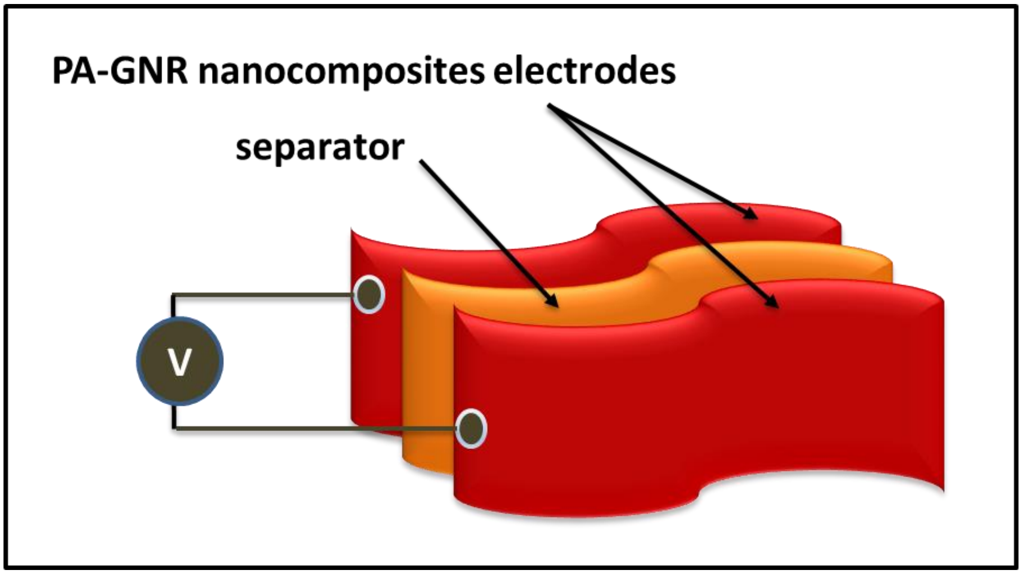

Figure 2.7: Schematic diagram of a quasi-solid state supercapacitor device.

CHAPTER III

RESULTS AND DISCUSSION

3.1. FT-IR analysis

The structural characterizations of the synthesized samples were performed using FT-IR spectroscopy. Figure 3.1 shows the FT-IR spectrum for CNT. No functional groups were detected in the FT-IR spectrum of CNT. After being unzipped, the obtained graphene nanoribbons exhibit distinguishing vibration peaks (Figure 3.2) which include: a broad and intense O-H peak at 3282 cm^{-1}, a strong C=O peak of carboxylic acid at 1740 cm^{-1}, C-O peak at 1367 cm^{-1}, a C-O-C peak at 1199 cm^{-1}, and a C-O stretching peak at 1041 cm^{-1} [25].

For pure PANI, as seen in Figure 3.3, several peaks were also observed. The peak at 1734 and 1550 cm^{-1} could be attributed to the C=C stretching of the quinoid ring and C=C stretching of the benzenoid ring, respectively. The peaks at 1367 and 1225 cm^{-1} could be ascribed to C–N stretching of the benzenoid unit and C–N stretching of the quinoid unit, respectively [26]. The peaks at 1054 and 932 cm^{-1} are attributed to the aromatic C-H bending both in and out of the plane for the 1,4-disubstituted aromatic ring [27].

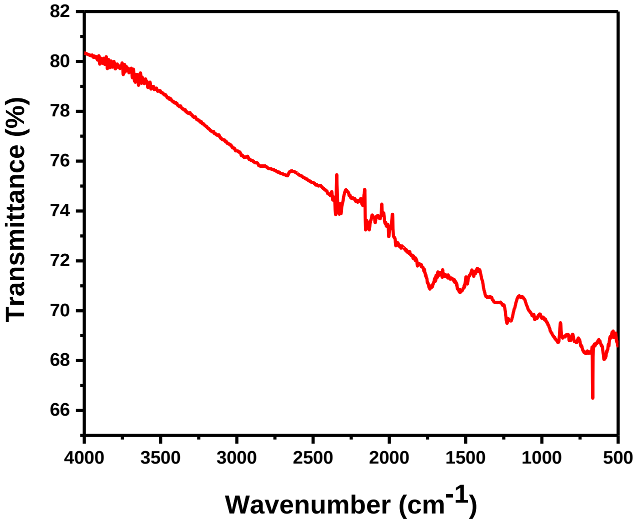

Figure 3.1: FT-IR spectra of CNT.

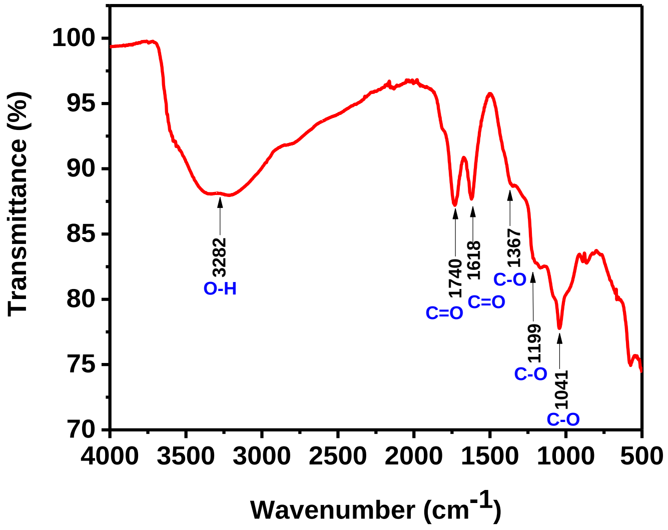

Figure 3.2: FT-IR spectra of GNRs.

FT-IR spectra of PANI-GNRs nanocomposite, in Figure 3.4-3.8, exhibited further evidence of interaction between GNR and PANI in the composites. Compared with that of PANI, the spectrum of PANI-GNR provided almost the same characteristic vibrations as PANI, but it was observed that some C–H bending peaks shifted to a higher wave number due to $\pi - \pi$ interaction and hydrogen bonding between the graphene sheets and PANI in the composites. This indicates that the PANI was deposited on the GNR's surface and chemically bounded [26].

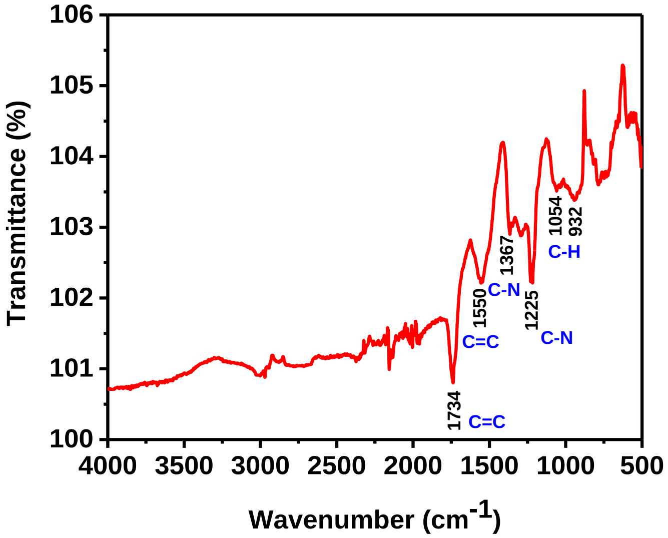

Figure 3.3: FT-IR spectra of polyaniline (PANI) sample.

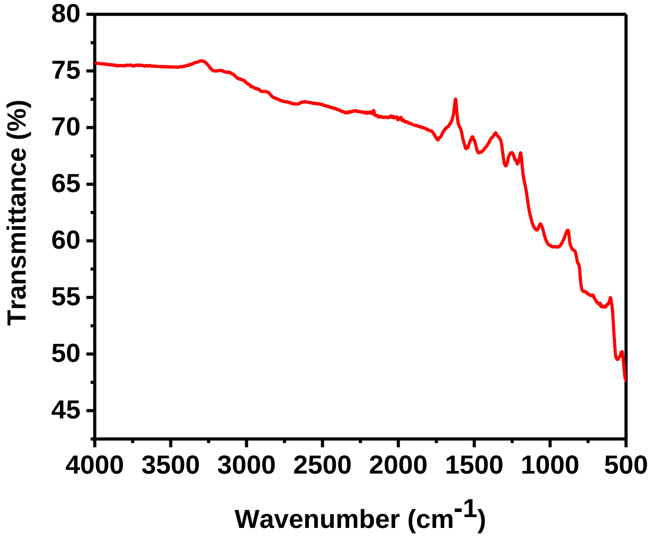

Figure 3.4: FT-IR spectra of PANI-GNR-105 sample.

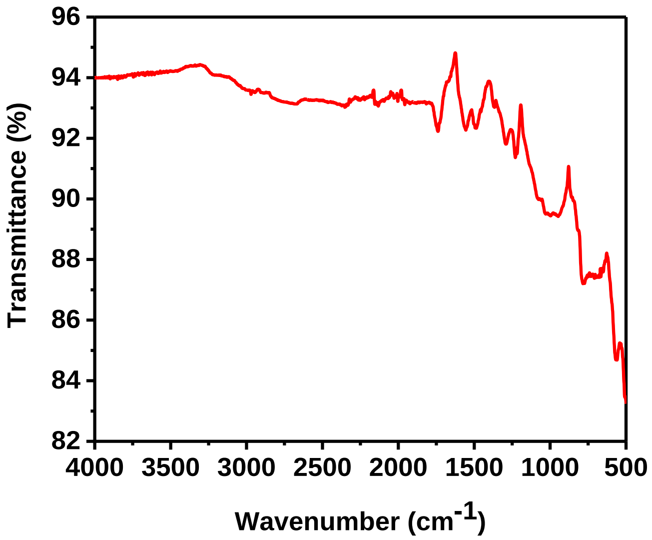

Figure 3.5: FT-IR spectra of PANI-GNR-106 sample.

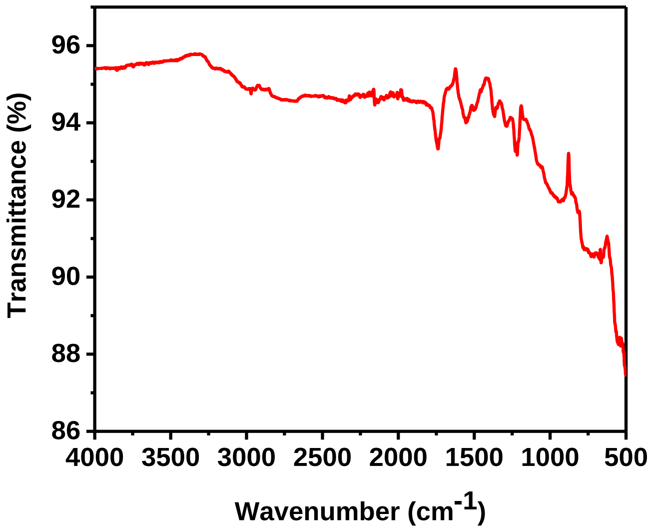

Figure 3.6: FT-IR spectra of PNAI-GNR-107 sample.

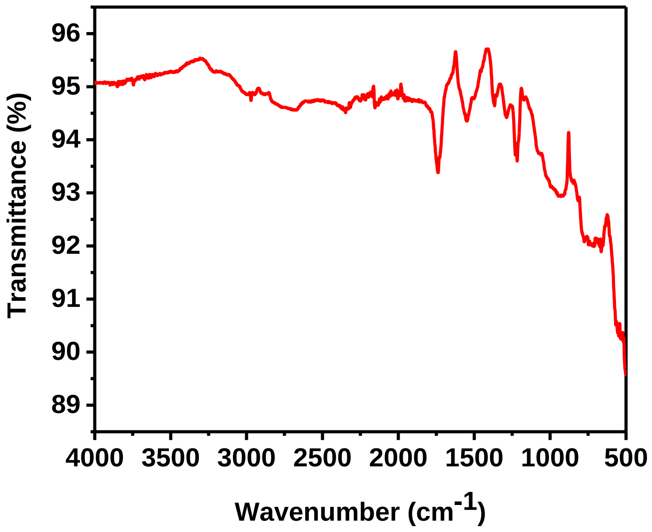

Figure 3.7: FT-IR spectra of PANI-GNR-108 sample.

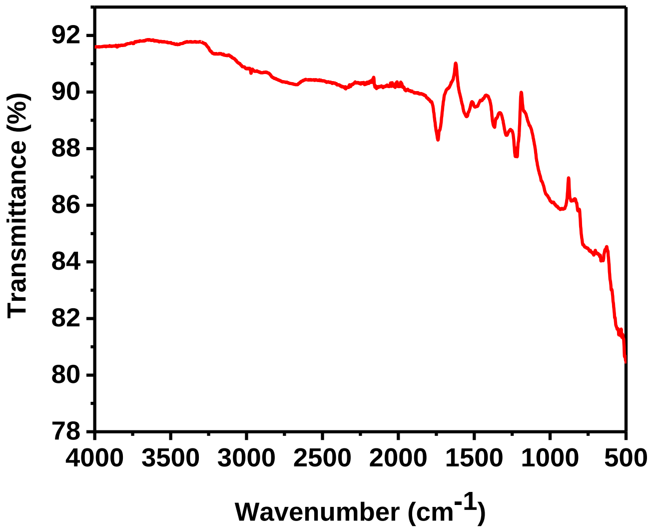

Figure 3.8: FT-IR spectra of PANI-GNR-109 sample.

3.2. X-ray diffraction analysis

X-ray diffraction (XRD) was also used to structurally characterize CNT, GNRs, PANI and nanocomposites of PANI-GNRs. It can be seen in Figure 3.9 that the XRD patterns of the CNT exhibit three diffraction peaks at two thetas of 26.4, 44.0 and 54.4, which corresponds to the graphite phase of the carbon. The GNR (Figure 3.10) showed a strong diffraction peak at 10.5, which can be indexed as (002) reflections of graphite; the other small peak around 44 is corresponding to (004). For pure PANI, as seen in Figure 3.11, the XRD patterns showed three characteristic peaks. The peaks at 15.3 and 25.4 are attributed to the periodicity, both perpendicular and parallel to the polymer chain, respectively. The peak at 20.8 resulted from the layers of polymer chains at alternating distances [28] In the XRD pattern of nanocomposite PANI-GNRs, most of the peaks correspond to pure polyaniline. This could be due to the addition of a very small amount of GNRs in the composites, which is not detectable using XRD.

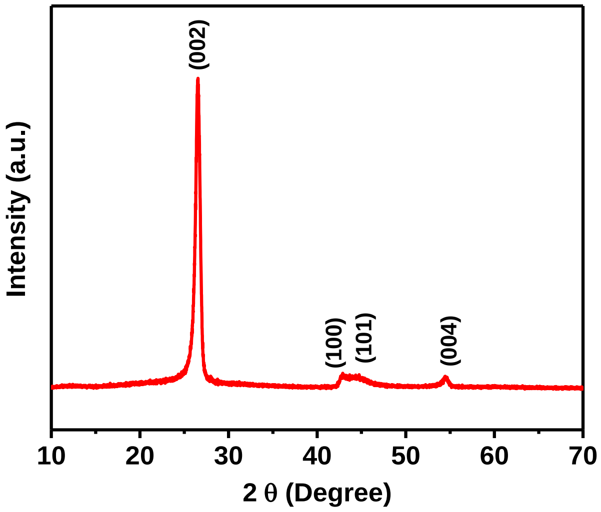

Figure 3.9: XRD patterns of CNT.

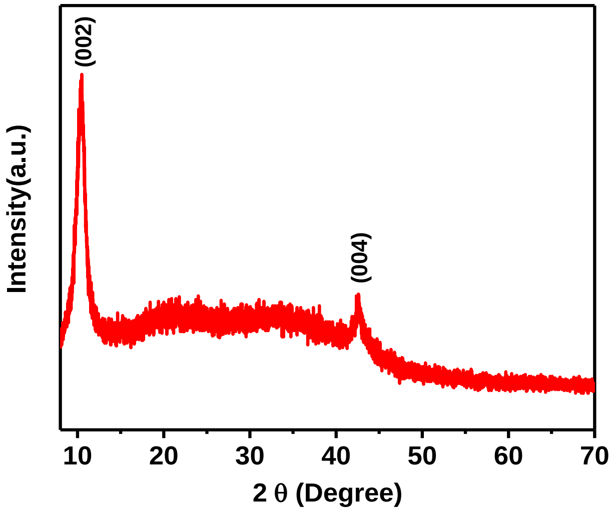

Figure 3.10: XRD pattern of GNRs.

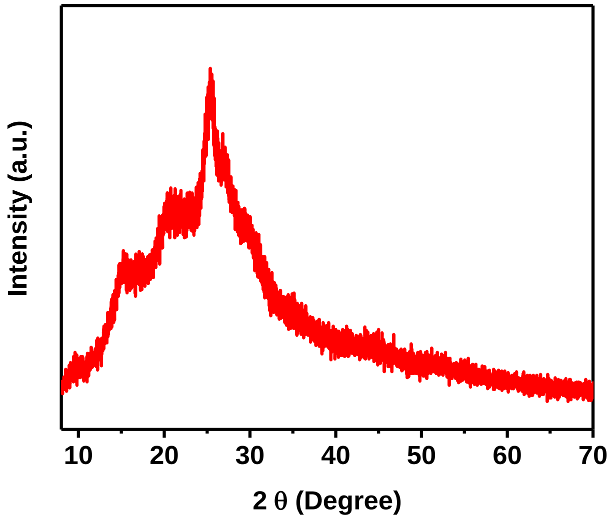

Figure 3.11: XRD pattern of polyaniline (PANI) sample.

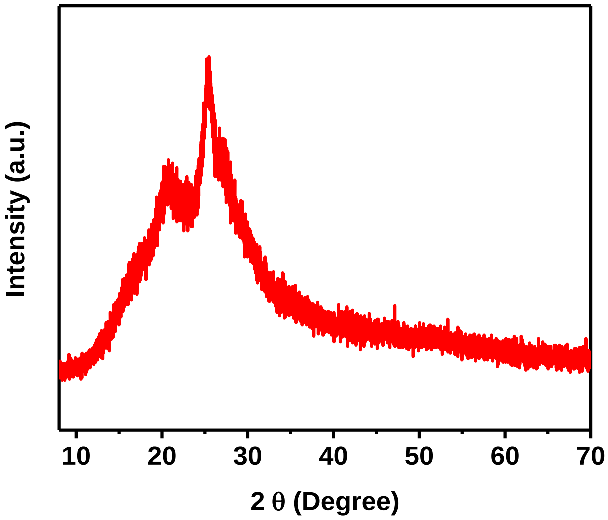

Figure 3.12: XRD pattern of PANI-GNR-105 sample.

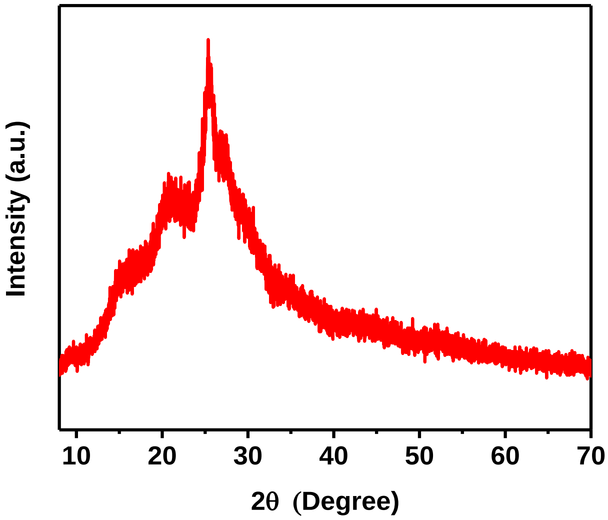

Figure 3.13: XRD pattern of PANI-GNR-106 sample.

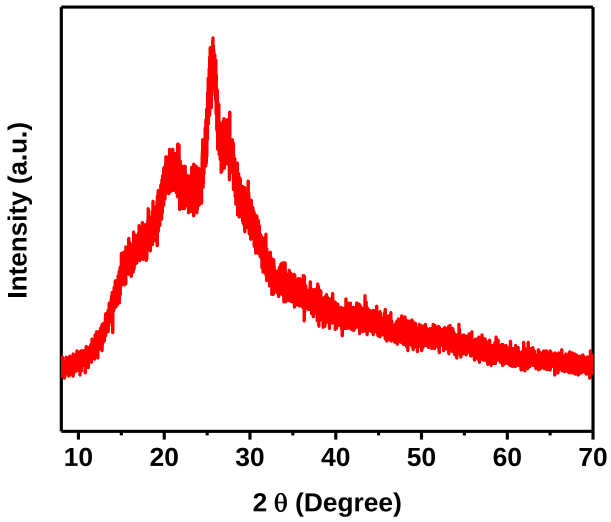

Figure 3.14: XRD pattern of PANI-GNR-107 sample.

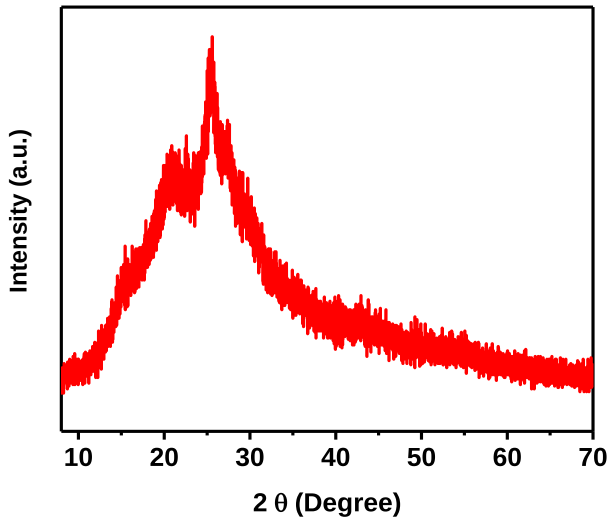

Figure 3.15: XRD pattern of PANI-GNR-108 sample.

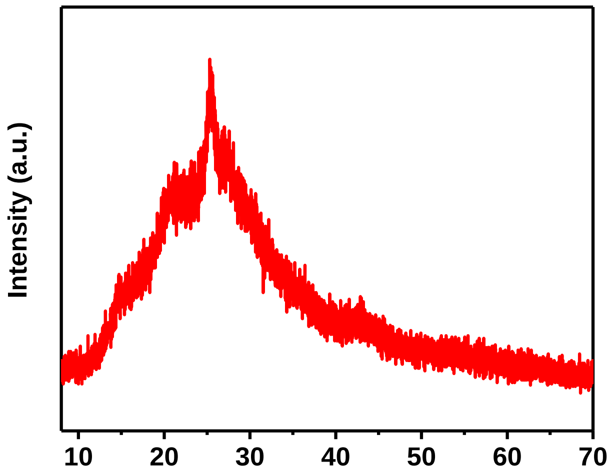

Figure 3.16: XRD pattern of PANI-GNR-109 sample.

3.3. Raman spectroscopy

The specific features of the GNRs, PANI and their polymeric nanocomposites were further analyzed using Raman spectroscopy. The Raman spectrum of GNRs is shown in Figure 3.17. As seen in the Raman spectrum of GNRs, two prominent peaks around 1354 cm^{-1} and 1596 cm^{-1} correspond to D and G peaks of carbon, respectively. The G peak represents the vibration of sp^2-hybridized carbon and the D peak corresponded to conversion of a sp^2-hybridized carbon to a sp^3-hybridized carbon [29]. The intensity of graphitic peak (G) is higher than the diamond phase peak (D), suggesting the GNRs are rich in graphitic phase. It is worth mentioning that the graphitic phase is the conducting form of the carbon whereas the diamond phase is non-conducting. The high percentage of conducting phase of carbon in GNR is favorable due to its ability to reduce the series resistance during the charging and discharging processes [30]. Raman spectrum of the pure polyaniline is shown in Figure 3.18. The peaks at 1241 and 1173 cm^{-1} correspond to the C-H bending vibrations of benzene and quinoid rings, respectively, while the peaks at 1554 and 1492 cm^{-1} correspond to C = C stretching vibrations of benzenoid and quinoid rings, respectively.

Figure 3.19 shows the Raman spectrum of the PANI-GNR-107 sample; the intensities of the two peaks were weakened, and that could be due to the strong interactions between the graphene and PANI.

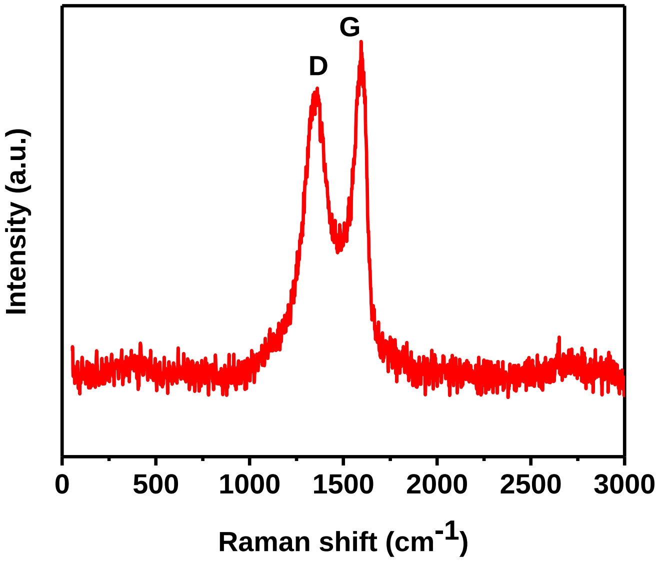

Figure 3.17: Raman spectrum of GNRs sample.

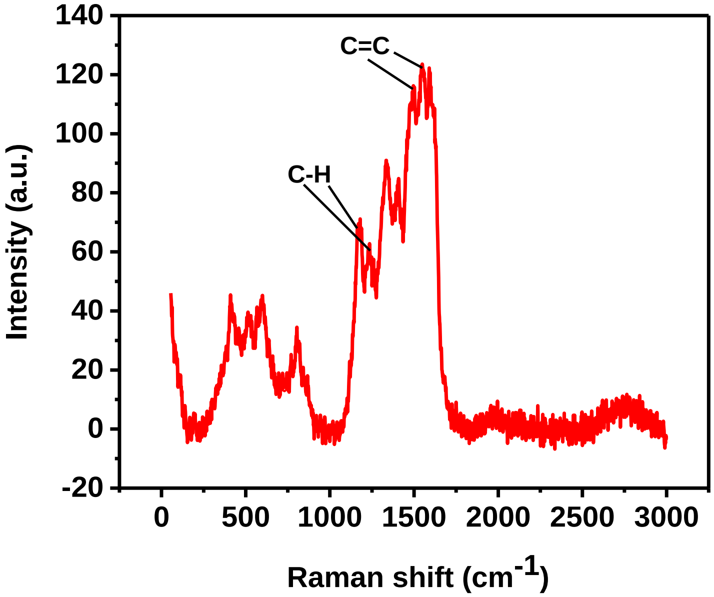

Figure 3.18: Raman spectrum of polyaniline sample.

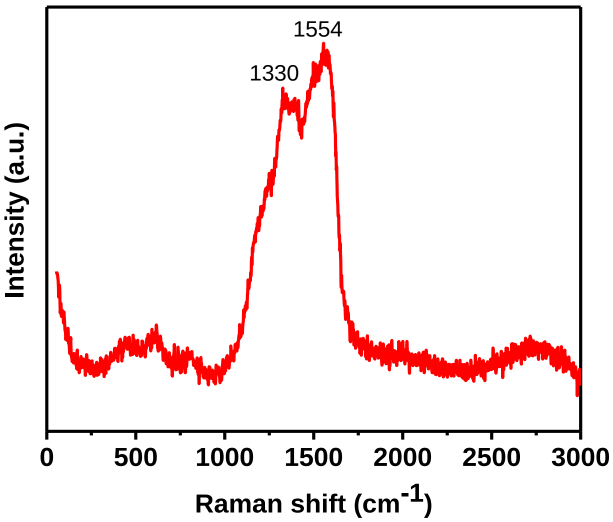

Figure 3.19: Raman spectrum of PANI-GNR-107 sample.

3.4. Scanning electron microscopic analysis

Scanning electron microscopy was used to investigate the morphology and structure of CNT, GNR, PANI and PANI-GNRs composites. Figure 3.20 shows the SEM images of carbon nanotubes at various magnifications. The GNRs synthesized from CNT is shown in Figure 3.21. It is seen that the tubular structure of CNT is changed to a sheet-like structure after unzipping it. Figure 3.22 demonstrates the porous structure for polyaniline without any graphene. Figures 3.23-3.27 show the SEM images of different nanocomposites of PANI-GNRs. As seen, the addition of small amounts of graphene in PANI does not change the structure of polyaniline significantly. However, higher amount of GNRs in the composites showed the presence of graphene sheets in the composites (Figure 3.26 and 3.27).

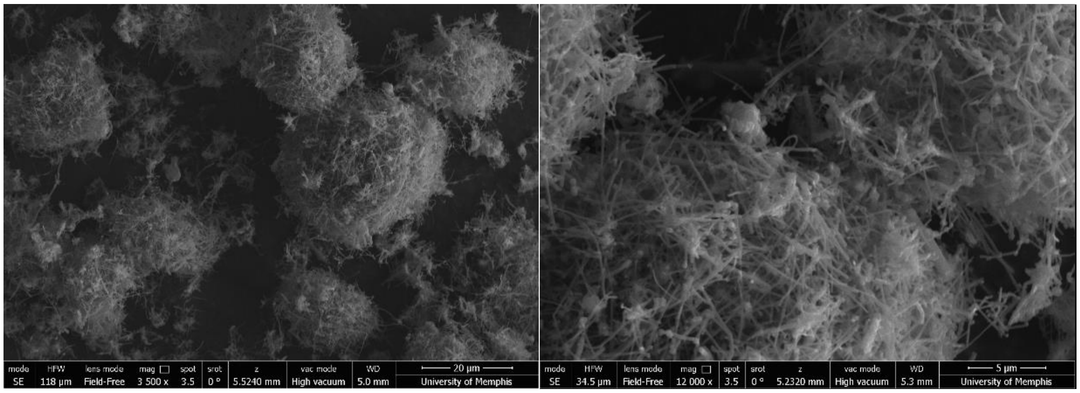

Figure 3.20: SEM images of CNT sample at various magnifications.

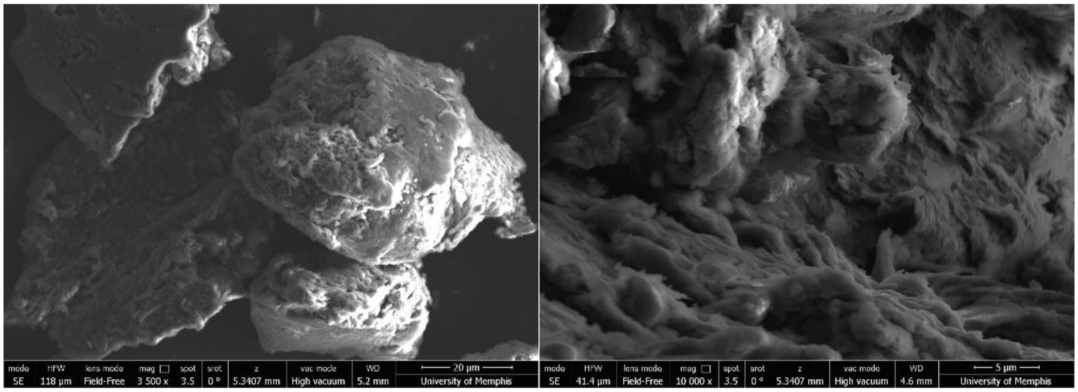

Figure 3.21: SEM images of GNRs sample at various magnifications.

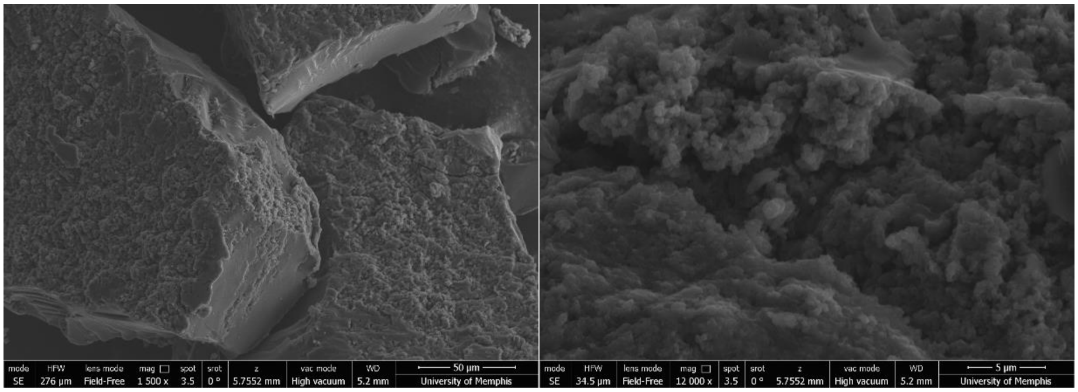

Figure 3.22: SEM images of PANI sample at various magnifications.

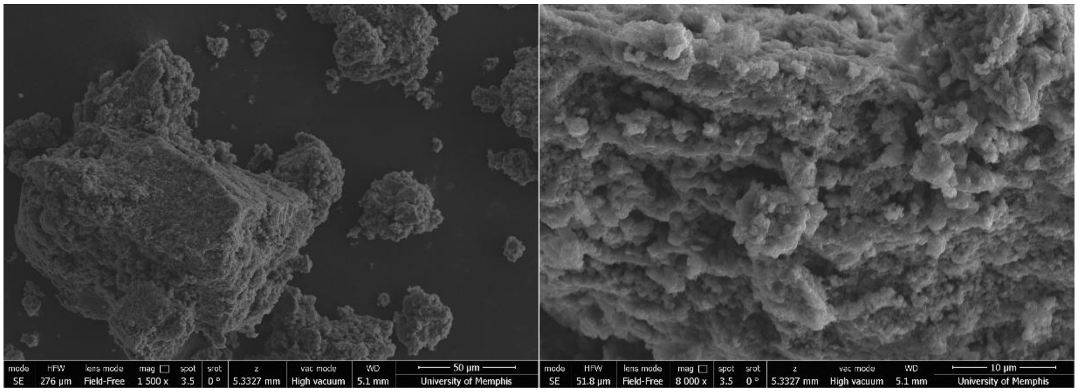

Figure 3.23: SEM images of PANI-GNR-105 sample at various magnifications.

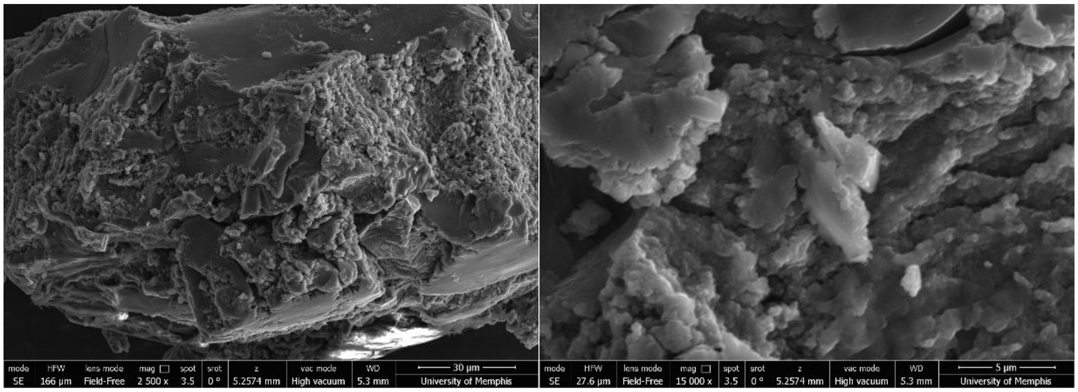

Figure 3.24: SEM images of PANI-GNR -106 sample at various magnifications.

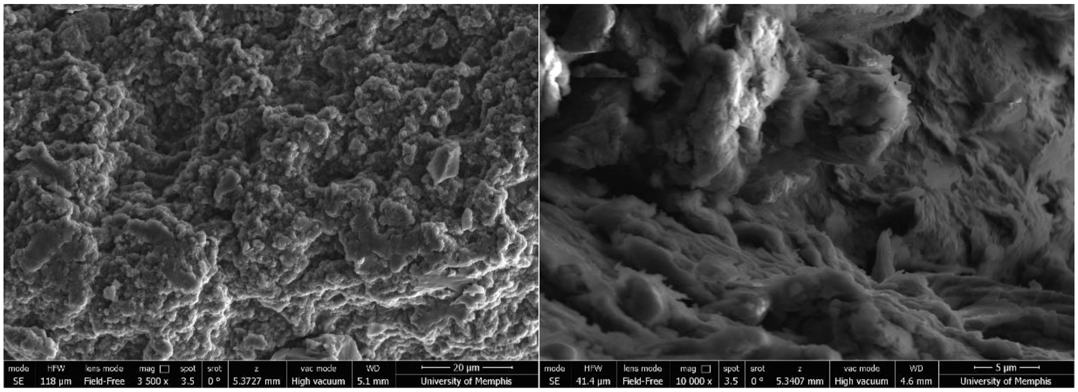

Figure 3.25: SEM images of PANI-GNR -107 sample at various magnifications.

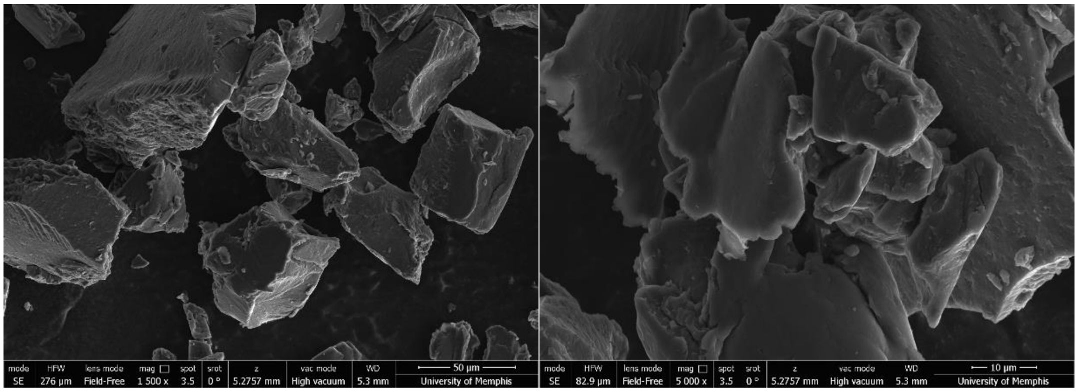

Figure 3.26: SEM images of PANI-GNR -108 sample at various magnifications.

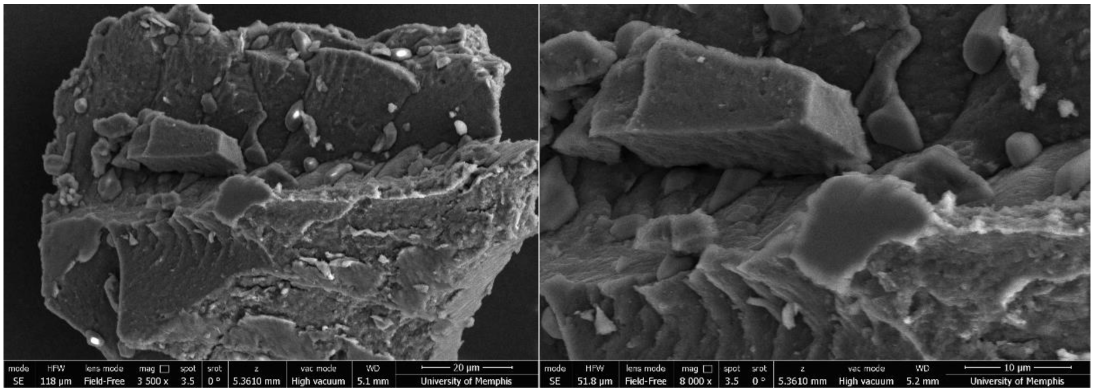

Figure 3.27: SEM images of PANI-GNR -109 sample at various magnifications.

3.5. Electrochemical measurements

3.5.1. Three-electrode system

Cyclic voltammetry (CV) and galvanostatic charge-discharge (GCD) measurements were performed to study the electrochemical properties of the synthesized graphene nanoribbons, polyaniline and their nanocomposites. The effects of scan rate and charge-discharge current density on the electrochemical properties of graphene nanoribbons, polyaniline and their nanocomposites were investigated in detail in 3M KOH electrolyte. Figure 3.28-3.36 show the cyclic voltammograms of CNT, GNR, PANI and PANI-GNRs nanocomposite samples at various scan rates. Comparing the electrochemical properties of CNT with GNR, it can be seen that GNR is better, which is due to the presence of more graphitic phase and high surface area through unzipping CNT. The CV curves of polyaniline at low scan rates show the presence of two pairs of redox peaks. These peaks correspond to doping and undoping of protons and anions in polyaniline and the transformation between different forms of polyaniline during a potential scan. At higher scan rates, these processes are merged, and only one pair of redox peaks were observed. In all the PANI-GNRs composites, one pair of redox peaks was also observed, indicating that redox process is the predominating mechanism for energy storage in these composites. It was observed that even at high scan rate, the CV curves are very similar, indicating high electrochemical rate stability of the synthesized materials. As stated earlier, the CV curves of CNT, GNR, PANI and PANI-GNRs nanocomposite showed a pair of redox peaks in oxidation and reduction process.

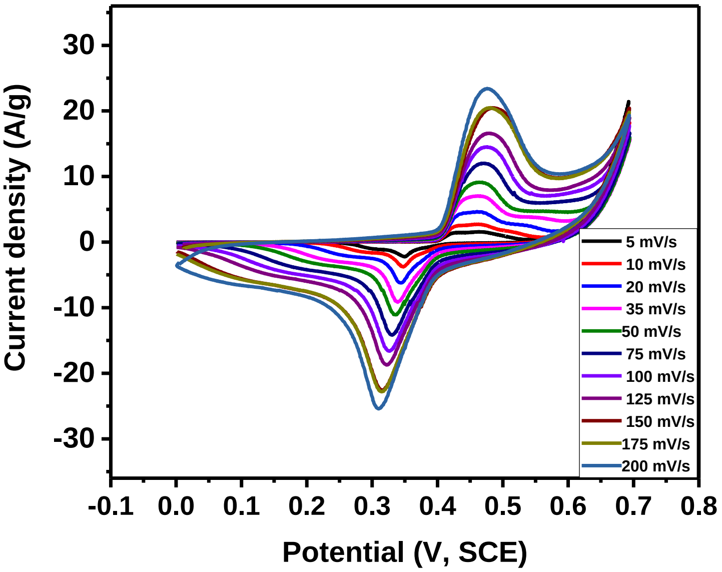

Figure 3.28: Cyclic voltammograms curves of CNT at various scan rates.

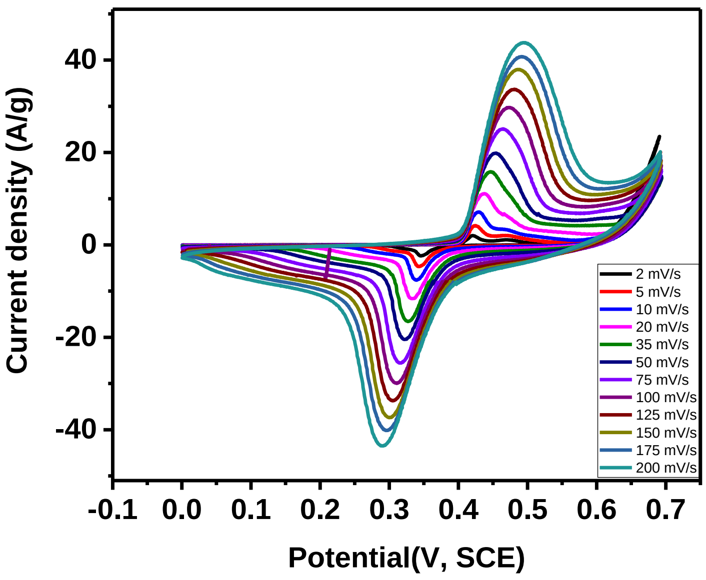

Figure 3.29: Cyclic voltammograms curves of GNRs at various scan rates.

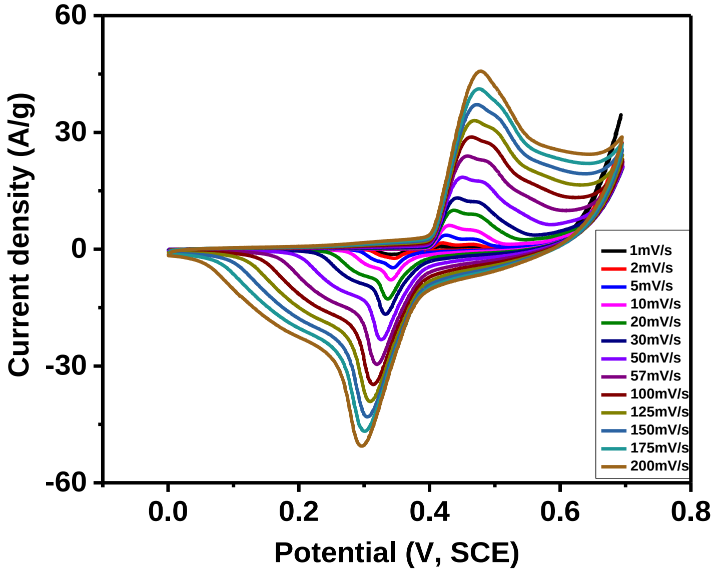

Figure 3.30: Cyclic voltammograms curves of polyaniline at various scan rates.

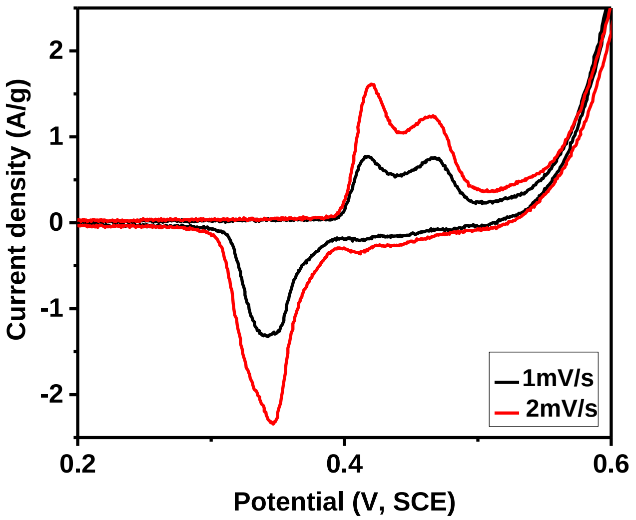

Figure 3.31: Cyclic voltammograms curves of polyaniline at low scan rates.

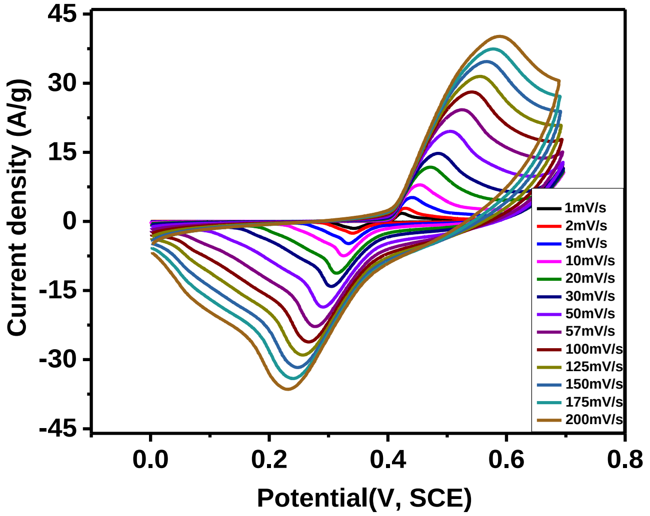

Figure 3.32: Cyclic voltammograms curves of PANI-GNR-105 at various scan rates.

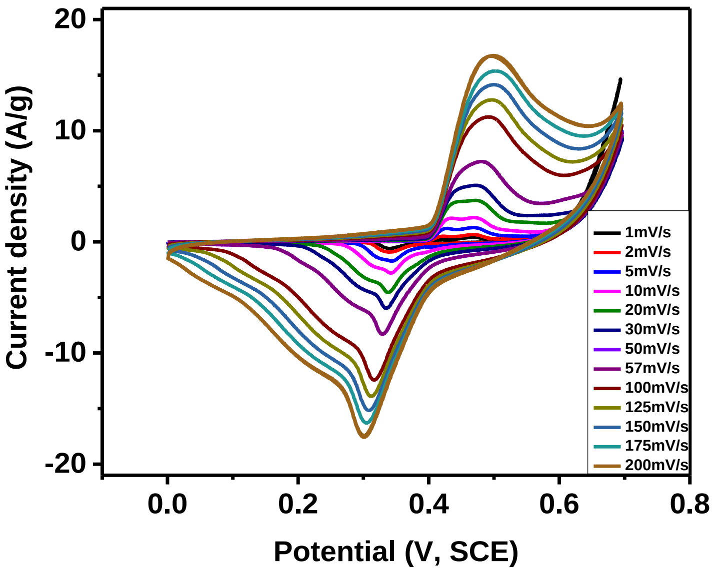

Figure 3.33: Cyclic voltammograms curves PANI-GNR-106 at various scan rates.

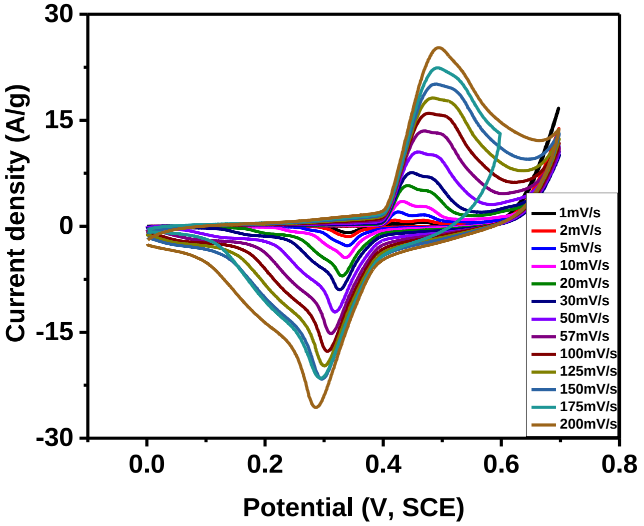

Figure 3.34: Cyclic voltammograms curves of PANI-GNR-107 at various scan rates.

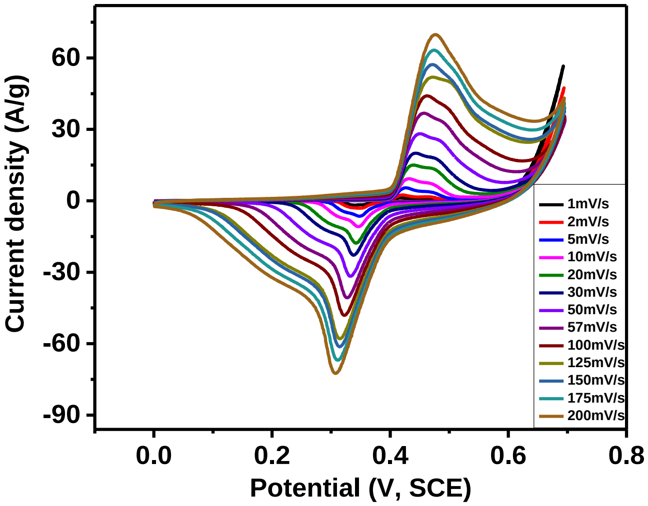

Figure 3.35: Cyclic voltammograms curves of PANI-GNR-108 at various scan rates.

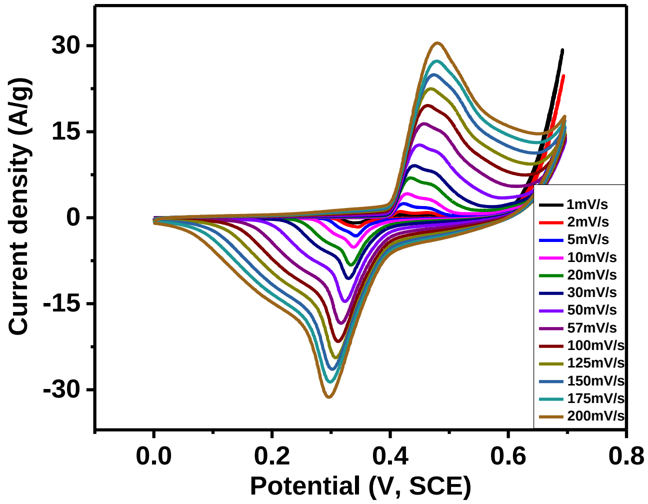

Figure 3.36: Cyclic voltammograms curves of PANI-GNR-109 at various scan rates.

Specific capacitance (Csp) of CNT, GNR, PANI and PANI-GNRs nanocomposites was calculated using data from the cyclic voltammetry measurements. The specific capacitance of as-prepared electrodes was calculated using the following expression [31]

$$Csp = Q/[\Delta V \times (\partial v / \partial t) \times m]$$

where Q is the area under the CV curve, $\partial v/\partial t$ is the scan rate, ΔV is the potential window and m is the mass of the sample used in the electrode. Figure 3.37-3.44 show the variation of specific capacitance as a function of scan rate for all the samples in the 3M KOH electrolyte. It was observed that the specific capacitance of the electrodes was decreasing with increasing scan rate in all the studied samples. The decrease in specific capacitance with increasing scan rate could be due to insufficient time for the redox reaction at the electrode. At a higher scan rate, the concentration of the ions at the electrode/electrolyte interface increases rapidly, and the diffusion rate of electrolyte from electrode/electrolyte interface to electrode will be not enough to satisfy the electrochemical reactions [32].The highest specific capacitance was observed for PANI-GNR-108 sample. The maximum specific capacitance of 7359 F/g was calculated for PANI-GNR-108 sample in 3M KOH electrolyte.

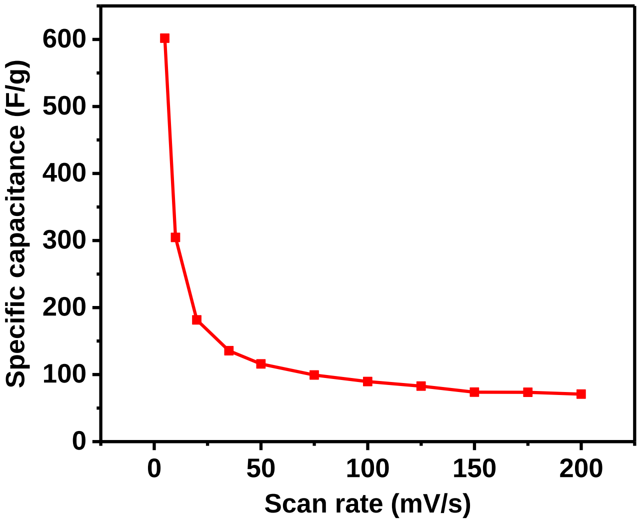

Figure 3.37: Specific capacitance as a function of scan rate for CNT.

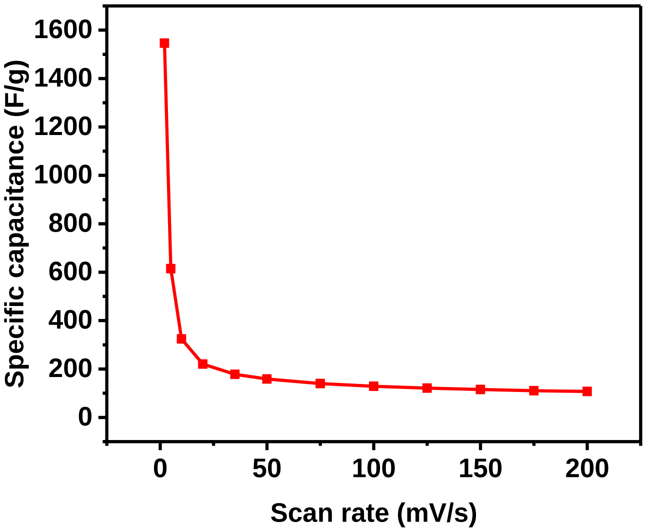

Figure 3.38: Specific capacitance as a function of scan rate for GNRs.

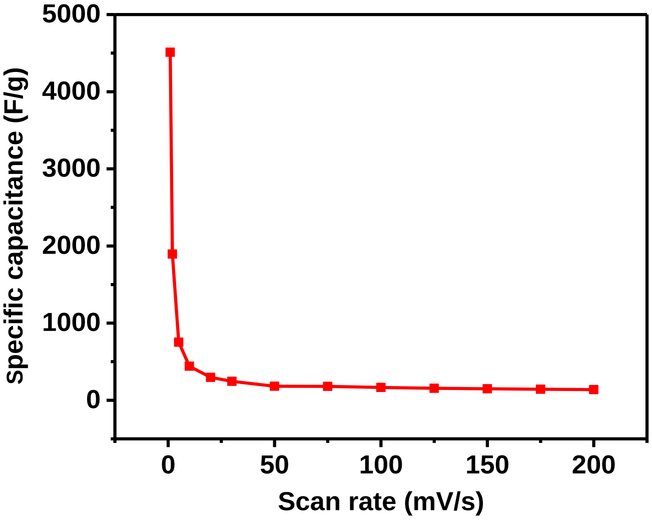

Figure 3.39: Specific capacitance as a function of scan rate for polyaniline.

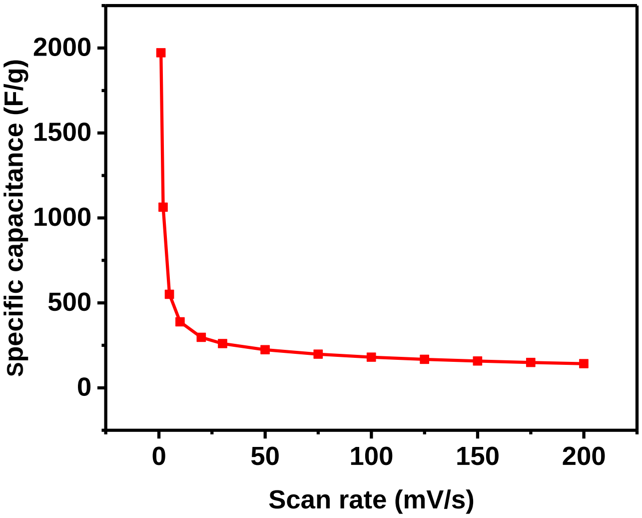

Figure 3.40: Specific capacitance as a function of scan rate for PANI-GNR-105.

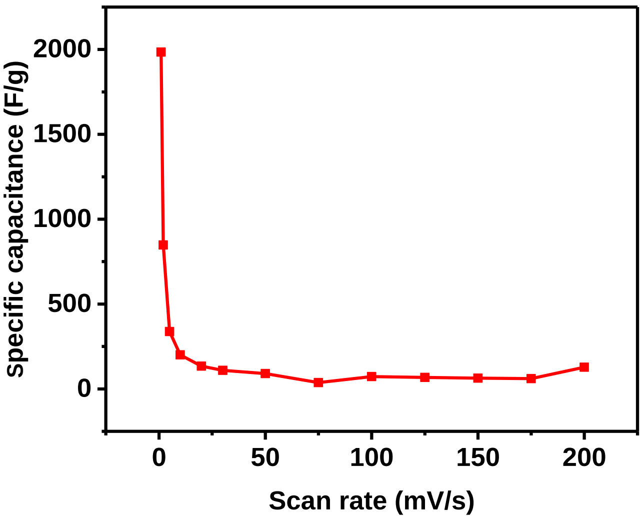

Figure 3.41: Specific capacitance as a function of scan rate for PANI-GNR-106.

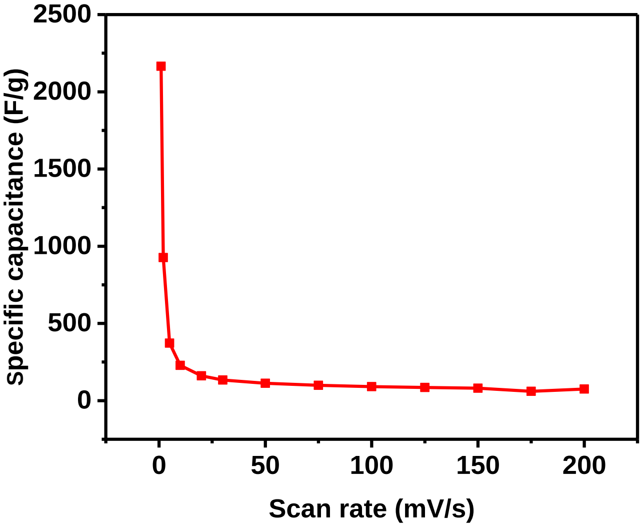

Figure 3.42: Specific capacitance as a function of scan rate for PANI-GNR-107.

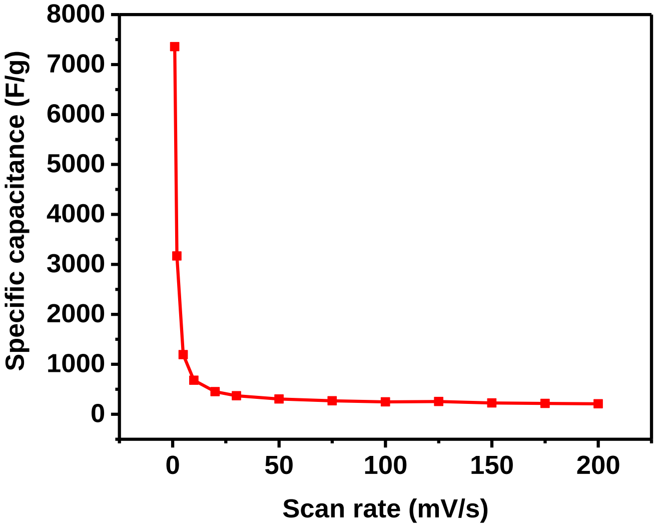

Figure 3.43: Specific capacitance as a function of scan rate for PANI-GNR-108.

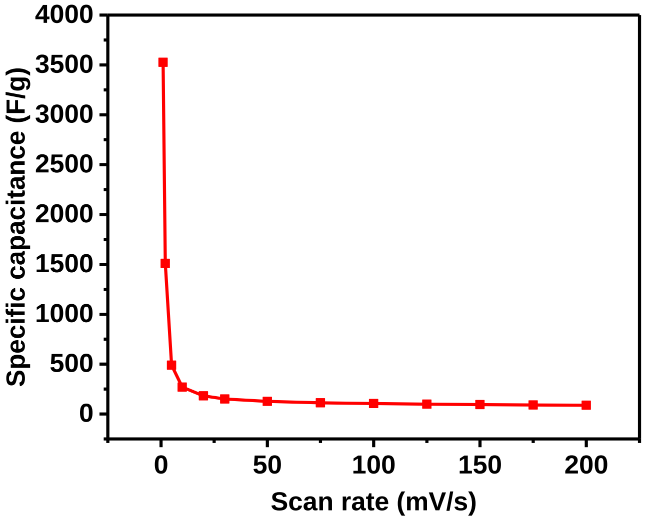

Figure 3.44: Specific capacitance as a function of scan rate PANI-GNR-109**.**

Galvanostatic charge-discharge measurements were performed to evaluate the potential application of the GNR, PANI and their nanocomposite as electrode materials for energy storage devices. The charge-discharge measurements were performed in 3M KOH electrolyte in a potential window of 0 to 0.6 V (vs. Saturated Calomel Electrode, SCE). Furthermore, charge-discharge studies were performed at various discharge current densities. The galvanostatic charge-discharge characteristics of the samples are shown in Figures 3.45-3.52. As seen, the discharge time decreases with an increase in discharge currents, indicating reduced charge storage capacity at higher current densities.

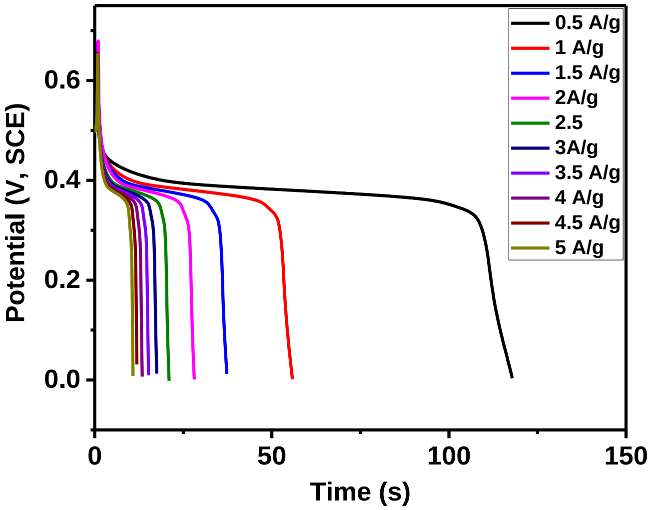

Figure 3.45: Galvanostatic charge-discharge characteristics of CNT electrode at various applied currents.

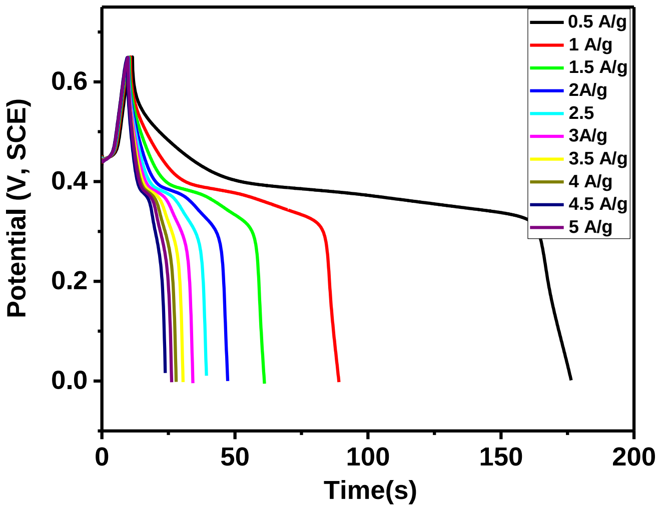

Figure 3.46: Galvanostatic charge-discharge characteristics of GNRs electrode at various applied currents.

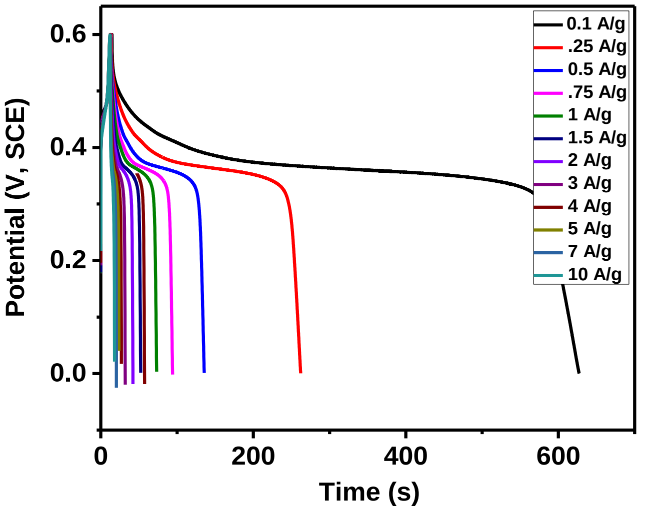

Figure 3.47: Galvanostatic charge-discharge characteristics of polyaniline electrode at various applied currents.

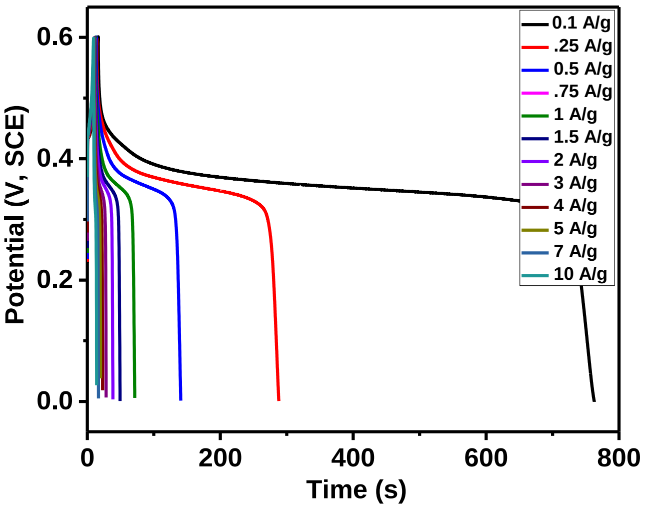

Figure 3.48: Galvanostatic charge-discharge characteristics of PANI-GNR-105 electrode at various applied currents.

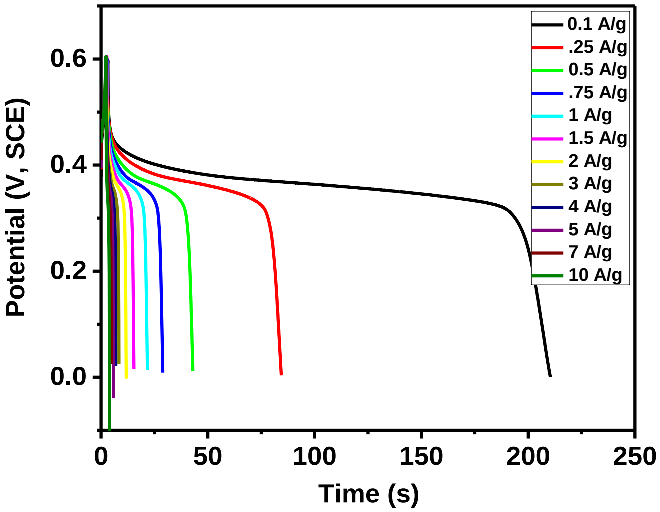

Figure 3.49: Galvanostatic charge-discharge characteristics of PANI-GNR-106 electrode at various applied currents.

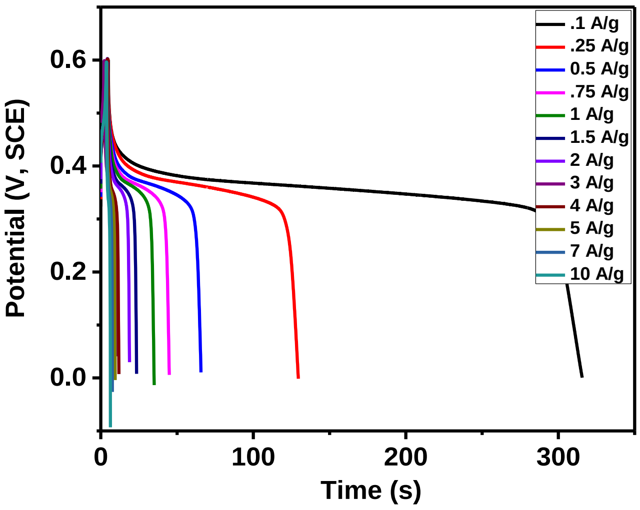

Figure 3.50: Galvanostatic charge-discharge characteristics of PANI-GNR-107 electrode at various applied currents.

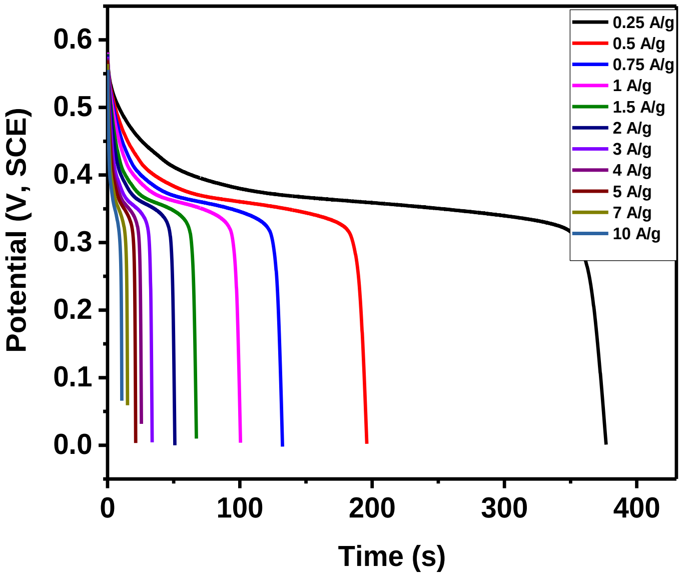

Figure 3.51: Galvanostatic charge-discharge characteristics of PANI-GNR-108 electrode at various applied currents.

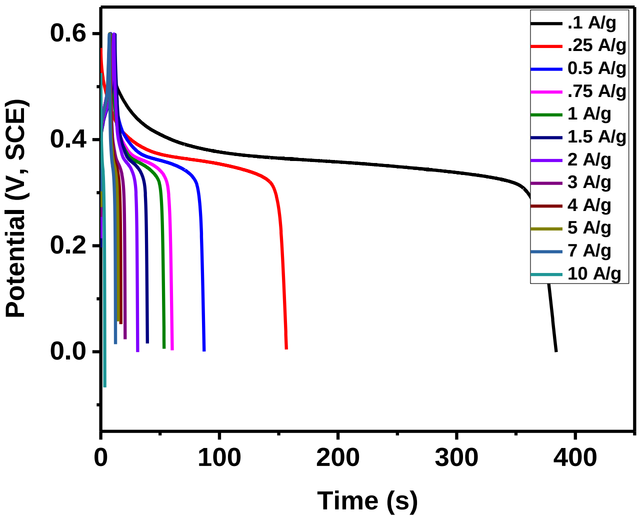

Figure 3.52: Galvanostatic charge-discharge characteristics of PANI-GNR-109 electrode at various applied currents.

The specific capacitance (Csp) of the electrodes was calculated from the discharging curves using the equation given below [33]:

$$Csp = I\times\Delta t/\Delta V\times m$$

where I is the discharge current (A), Δt is the discharge time (s), ΔV is the potential window (V) and m is the mass of the active materials. It was observed that the specific capacitances of all the electrodes decrease when discharge current is increased (Figures 3.53-3.60). The decrease in specific capacitance with the increase of the discharge current is due to the increase of potential drop and insufficient Faradic redox reaction at higher discharge currents [34].

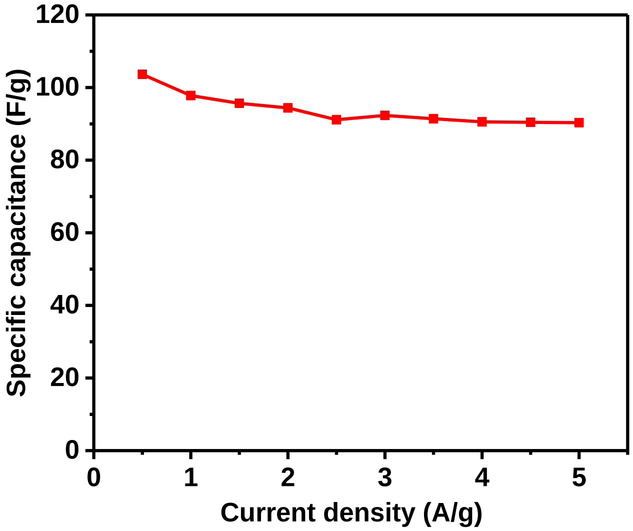

Figure 3.53: Variation of specific capacitance with applied current for CNT sample.

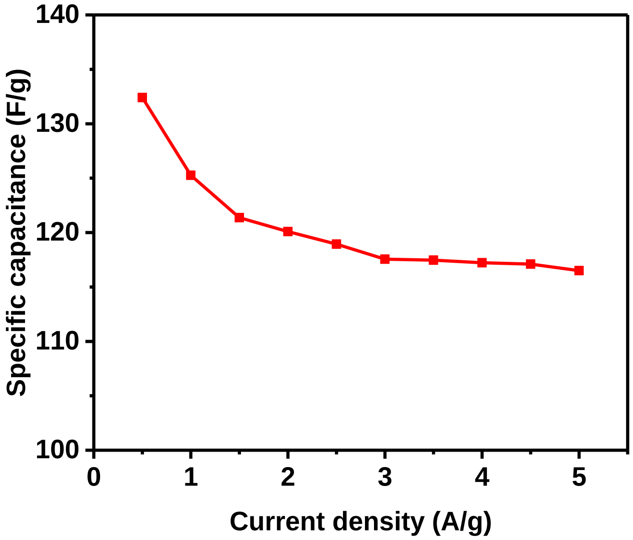

Figure 3.54: Variation of specific capacitance with applied current for GNRs sample.

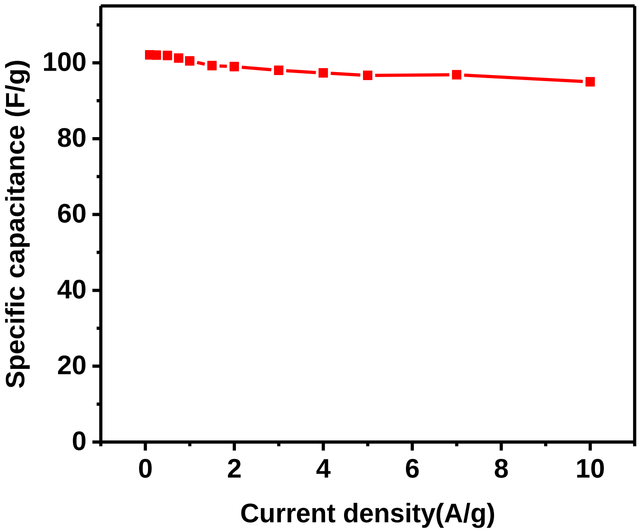

Figure 3.55: Variation of specific capacitance with applied current in for polyaniline sample.

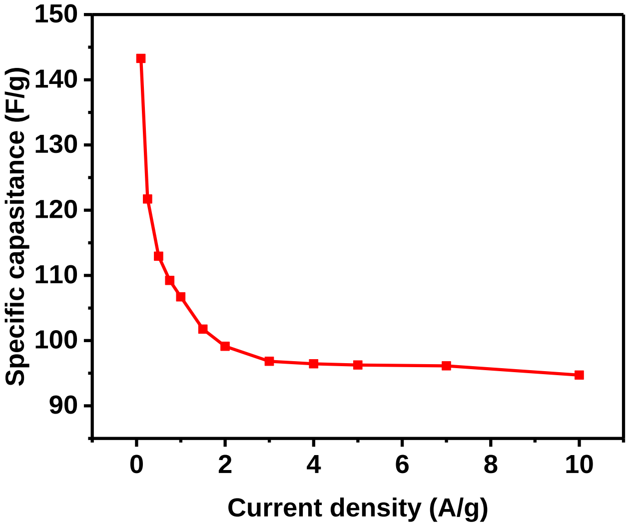

Figure 3.56: Variation of specific capacitance with applied current for PANI-GNR-105.

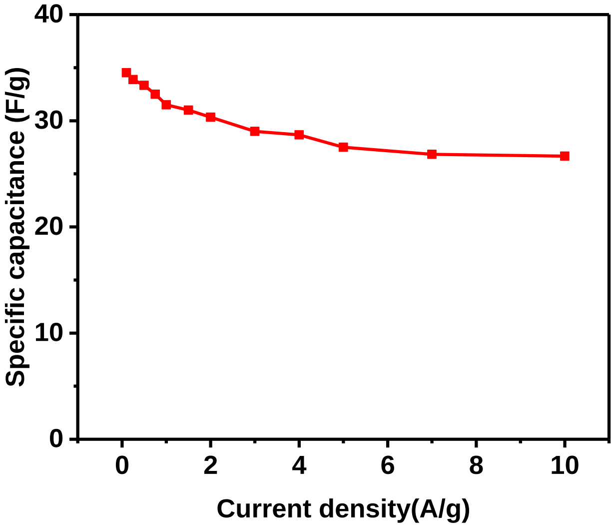

Figure 3.57: Variation of specific capacitance with applied current for PANI-GNR-106.

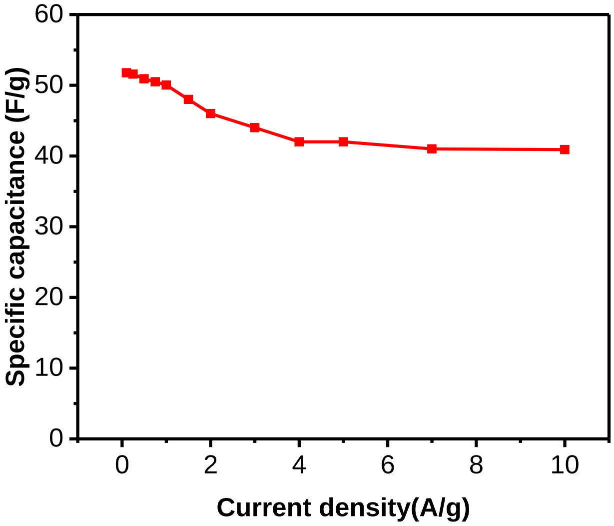

Figure 3.58: Variation of specific capacitance with applied current for PANI-GNR-107.

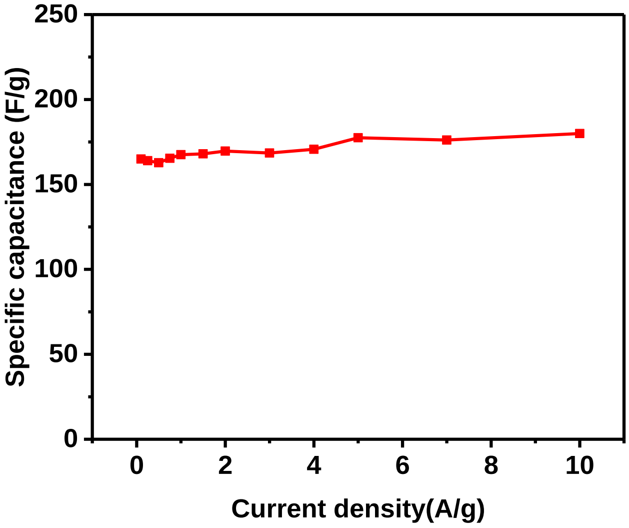

Figure 3.59: Variation of specific capacitance with applied current for PANI-GNR-108.

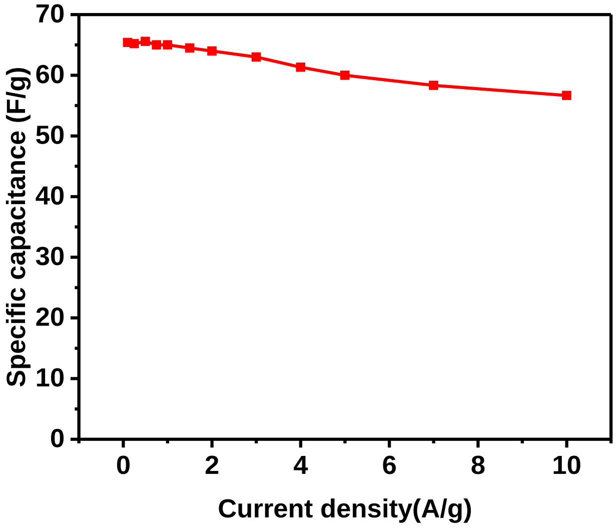

Figure 3.60: Variation of specific capacitance with applied current for PANI-GNR-109.

3.5.2. Electrochemical characteristics of the supercapacitor device

For the potential applications, a supercapacitor device was fabricated by sandwiching an ion-transporting layer between two PA-GNR-108 electrodes. The device was prepared in 3M KOH electrolyte to study the electrochemical properties. The effect of scan rate on the charge storage capacity of the device at room temperature and at elevated temperatures was investigated. Figure 3.61 shows the cyclic voltammetry curves of the device at room temperature at different scan rates. As observed from the curves, the shape of the CV curve is nearly identical even at higher scan rates, indicating high electrochemical stability of the fabricated device. Additionally, the CV curves are nearly rectangular in shape, suggesting near ideal capacitive behavior of the fabricated device.

The percentage change in the specific capacitance of the device as a function of temperature is shown in Figure 3.62. A roughly 112 % improvement in the charge storage capacity of the device was observed by increasing temperature from 10°C to 70°C. The improved performance at higher temperatures could be due to higher mobility of electrolyte ions and low series resistance of the device. Based on the results, it can be concluded that the supercapacitor device based on PANI-GNR nanocomposites could be used in a wide temperature range.

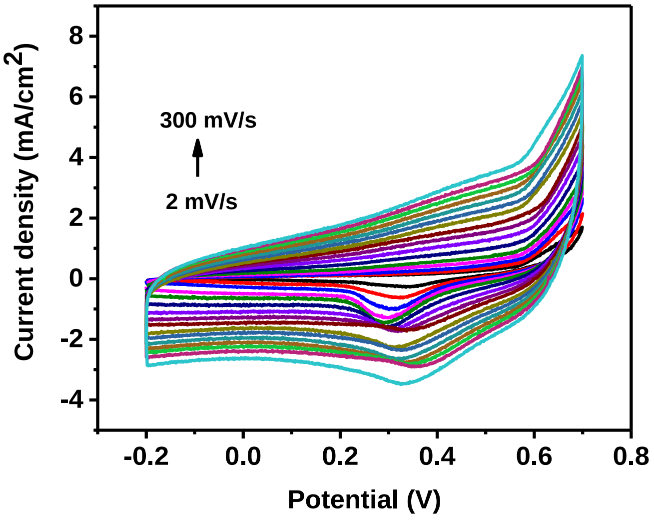

Figure 3.61: Cyclic voltammograms curves of the device at room temperatures at various scan rates.

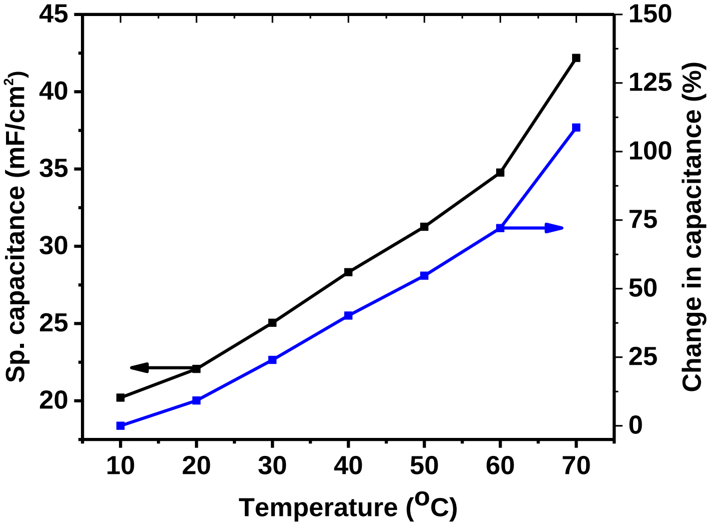

Figure 3.62: Specific capacitance of the device versus temperatures and % change in specific capacitance of the device versus temperatures.

The electrochemical impedance spectroscopy (EIS) of the device at various temperatures was studied to better understand the charge storage process in the device. Figure 3.63 shows the variation of real and imaginary impedance (Nyquist plots) of the device at various temperatures. It was observed that the real and imaginary impedance of the device decreases with an increase in temperature. Figure 3.64 shows the zoomed part of the Nyquist plots near the high frequency range at various temperatures. As seen in Figure 3.64, the series resistance of the device decreases with an increase in temperature, which improves the charge storage capacity at higher temperatures. The variation of total impedance with frequency at various temperatures (Figure 3.65) shows that impedance of the device decreases with increase in frequency at lower frequencies, while impedance is almost constant at higher frequencies. The lower impedance at higher temperatures is due to high mobility of the electrolyte and reduced series resistance of the device.

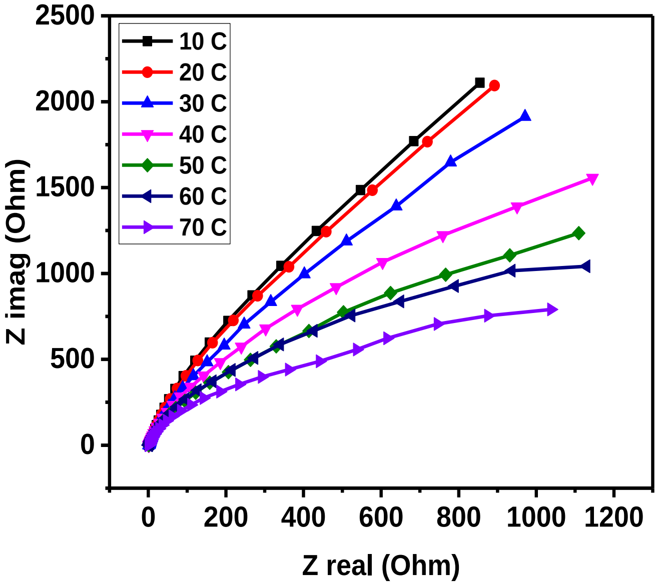

Figure 3.63: Nyquist plots of the device at various temperatures.

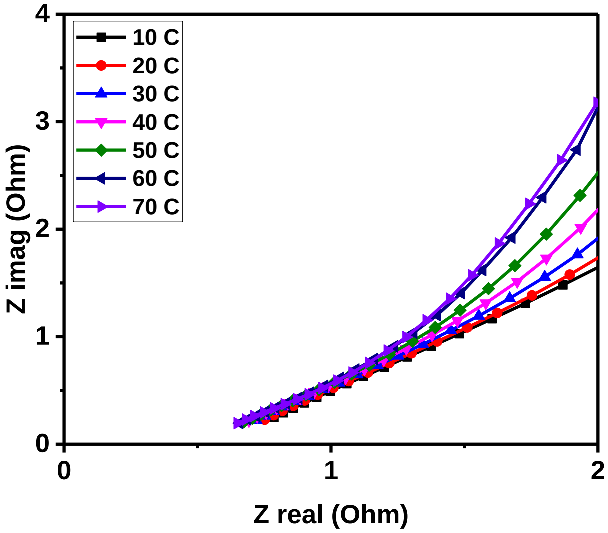

Figure 3.64: Nyquist plots of the device zoomed near origin at various temperatures.

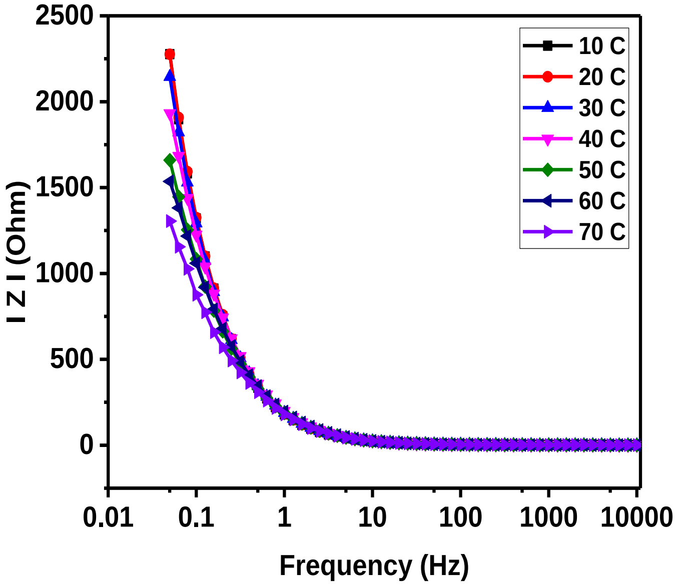

Figure 3.65: Variation of impedance of the device as a function of frequency at various temperatures.

CHAPTER IV

CONCLUSION

Graphene nanoribbons were synthesized by unzipping carbon nanotubes using a chemical method. Unzipping these carbon nanotubes (graphene nanoribbons) showed a shift in the lattice parameter compared with pure carbon nanotubes. This result indicated that this chemical process exfoliates the unzipped carbon nanotubes too. The graphene nanoribbons were used to synthesize nanocomposites with polyaniline. The synthesized graphene nanoribbons, polyaniline, and their nanocomposites were structurally and electrochemically characterized. The FT-IR studies indicated that graphene nanoribbons are functionalized, which make them disperse well in an aqueous solution. The Raman spectra confirms the presence of both diamond and graphite phases of the carbon. The microstructural analysis using scanning electron microscopy indicated a nanostructure nature of the composites with a homogenous mixture of the components. It was observed that the electrochemical properties of the nanocomposites are better than pure polyaniline and graphene nanoribbons. The energy storage capacity increased with an increase in amount of graphene nanoribbons, and then began to decrease with further increase. The maximum specific capacitance was observed for the nanocomposite having 5 wt% of graphene nanoribbons. A quasi-solid supercapacitor device was fabricated using two PA-GNR-108 electrodes. The CV curve of the fabricated device was nearly rectangular in shape, suggesting near ideal capacitive behavior of the fabricated device. The effect of temperature on the energy storage capacity was studied; it was observed that the energy storage performance increased by about 110% by increasing the temperature from 10 to 70 ^{o}C. The improved performance at a higher temperature was explained on the basis of series resistance and impedance of the device. Our study suggests that nanocomposites of polyaniline and graphene nanoribbons could be a potential material for energy storage applications.

REFERENCES V

(1) Burke, A. Ultracapacitors: Why, How, and Where Is the Technology. *J. Power Sources* **2000**, *91* (1), 37–50.

(2) Conway, B. E. Transition from “Supercapacitor” to “Battery” Behavior in Electrochemical Energy Storage. *J. Electrochem. Soc.* **1991**, *138* (6), 1539.

(3) Conway, B. E.; Pell, W. G. Double-Layer and Pseudocapacitance Types of Electrochemical Capacitors and Their Applications to the Development of Hybrid Devices. *J. Solid State Electrochem.* **2003**, *7* (9), 637–644.

(4) Ryu, K. S.; Kim, K. M.; Park, N.-G.; Park, Y. J.; Chang, S. H. *Symmetric Redox Supercapacitor with Conducting Polyaniline Electrodes*; 2002; Vol. 103.

(5) Yuan, A.; Zhang, Q. *A Novel Hybrid Manganese Dioxide/activated Carbon Supercapacitor Using Lithium Hydroxide Electrolyte*; 2006; Vol. 8.

(6) Halper, M.S. and J.C. Ellenbogen, *Supercapacitors: A brief overview.* The MITRE Corporation, McLean, Virginia, USA, **2006**: 1-34.

(7) Laforgue, A.; Simon, P.; Fauvarque, J. F.; Mastragostino, M.; Soavi, F.; Sarrau, J. F.; Lailler, P.; Conte, M.; Rossi, E.; Saguatti, S. Activated Carbon/Conducting Polymer Hybrid Supercapacitors. *J. Electrochem. Soc.* **2003**, *150* (5), A645.

(8) Choi, H. S.; Kim, T.; Im, J. H.; Park, C. R.; Amatucci G G, B. F. P. A. D. and Z. T.; Arico A S, B. P. S. B. T. J. M. and V. S. W.; Brousse T, M. R. T. P. L. and S. P.; M, B. A. and M.; Chen J Z, Y. L. F. S. H. and T. Y. F.; Cheng L, L. X. L. L. H. J. X. H. M. Z. P. W. and X. Y. Y.; et al. Preparation and Electrochemical Performance of Hyper-Networked $Li_4Ti_5O_{12}$ / Carbon Hybrid Nanofiber Sheets for a Battery–supercapacitor Hybrid System. *Nanotechnology* **2011**, *22* (40), 405402.

(9) Wang, Q.; Wen, Z. H.; Li, J. H. A Hybrid Supercapacitor Fabricated with a Carbon Nanotube Cathode and a TiO2–B Nanowire Anode. *Adv. Funct. Mater.* **2006**, *16* (16), 2141–2146.

(10) Obreja, V. V. N. On the Performance of Supercapacitors with Electrodes Based on Carbon Nanotubes and Carbon Activated material—A Review. *Phys. E Low-dimensional Syst. Nanostructures* **2008**, *40* (7), 2596–2605.

(11) Mellor, P. H. Flywheel and Supercapacitor Peak Power Buffer Technologies. In *IEE Seminar on Electric, Hybrid and Fuel Cell Vehicles*; IEE, 2000; Vol. 2000, pp 8–8.

(12) Ongaro, F.; Saggini, S.; Mattavelli, P. Li-Ion Battery-Supercapacitor Hybrid Storage System for a Long Lifetime, Photovoltaic-Based Wireless Sensor Network. *IEEE Trans. Power Electron.* **2012**, *27* (9), 3944–3952.

(13) Picó, F.; Rojo, J. M.; Sanjuán, M. L.; Ansón, A.; Benito, A. M.; Callejas, M. A.; Maser, W. K.; Martínez, M. T. Single-Walled Carbon Nanotubes as Electrodes in Supercapacitors. *J. Electrochem. Soc.* **2004**, *151* (6), A831.

(14) Frackowiak, E.; Metenier, K.; Bertagna, V.; Beguin, F. Supercapacitor Electrodes from Multiwalled Carbon Nanotubes. *http://dx.doi.org/10.1063/1.1290146* **2000**.

(15) Xie, X.; Gao, L. Characterization of a Manganese Dioxide/carbon Nanotube Composite Fabricated Using an in Situ Coating Method. *Carbon N. Y.* **2007**, *45* (12), 2365–2373.

(16) Wenelska, K.; Neef, C.; Schlestein, L.; Klingeler, R.; Kalenczuk, R. J.; Mijowska, E. Carbon Nanotubes Decorated by Mesoporous Cobalt Oxide as Electrode Material for Lithium-Ion Batteries. *Chem. Phys. Lett.* **2015**, *635*, 185–189.

(17) Kaner, R. B. Graphene-Based Supercapacitors.

(18) Agrawal, R., Chen, C., Hao, Y., Song, Y. & Wang, C., *Graphene for supercapacitors.* Graphene-based Energy Devices, **2015**: p. 171-214

(19) Kötz, R.; Carlen, M. Principles and Applications of Electrochemical Capacitors. *Electrochim. Acta* **2000**, *45* (15), 2483–2498.

(20) Jurewicz, K.; Babeł, K.; Pietrzak, R.; Delpeux, S.; Wachowska, H. Capacitance Properties of Multi-Walled Carbon Nanotubes Modified by Activation and Ammoxidation. *Carbon N. Y.* **2006**, *44* (12), 2368–2375.

(21) Frackowiak, E.; Béguin, F. Electrochemical Storage of Energy in Carbon Nanotubes and Nanostructured Carbons. *Carbon N. Y.* **2002**, *40* (10), 1775–1787.

(22) Zhang, K.; Zhang, L. L.; Zhao, X. S.; Wu, J. Graphene/Polyaniline Nanofiber Composites as Supercapacitor Electrodes. *Chem. Mater.* **2010**, *22* (4), 1392–1401.

(23) Wu, Q.; Xu, Y.; Yao, Z.; Liu, A.; Shi, G. Supercapacitors Based on Flexible Graphene/Polyaniline Nanofiber Composite Films. *ACS Nano* **2010**, *4* (4), 1963–1970.

(24) Peng, C.; Zhang, S.; Jewell, D.; Chen, G. Z. Carbon Nanotube and Conducting Polymer Composites for Supercapacitors. *Prog. Nat. Sci.* **2008**, *18* (7), 777–788.

(25) Si, Y.; Samulski, E. T. Synthesis of Water Soluble Graphene. *Nano Lett.* **2008**, *8* (6), 1679–1682.

(26) Dong, Y.; Zhou, Y.; Ding, Y.; Chu, X.; Wang, C.; Bodo, M.; Balloni, S.; Lumare, E.; Bacci, M.; Calvitti, M.; et al. Sensitive Detection of Pb(Ii) at Gold Nanoparticle/polyaniline/graphene Modified Electrode Using Differential Pulse Anodic Stripping Voltammetry. *Anal. Methods* **2014**, *6* (23), 9367–9374.

(27) Yan, X. B.; Han, Z. J.; Yang, Y.; Tay, B. K. NO 2 Gas Sensing with Polyaniline Nanofibers Synthesized by a Facile Aqueous/organic Interfacial Polymerization. *Sensors Actuators B* **2007**, *123*, 107–113.

(28) Li, Y.; Zhao, X.; Yu, P.; Zhang, Q. Oriented Arrays of Polyaniline Nanorods Grown on Graphite Nanosheets for an Electrochemical Supercapacitor. *Langmuir* **2013**, *29* (1), 493–

500.

(29) Kudin, K. N.; Ozbas, B.; Schniepp, H. C.; Prud'homme, R. K.; Aksay, I. A.; Car, R. Raman Spectra of Graphite Oxide and Functionalized Graphene Sheets. *Nano Lett.* **2008**, *8* (1), 36–41.

(30) Zequine, C.; Ranaweera, C. K.; Wang, Z.; Singh, S.; Tripathi, P.; Srivastava, O. N.; Gupta, B. K.; Ramasamy, K.; Kahol, P. K.; Dvornic, P. R.; et al. High Per Formance and Flexible Supercapacitors Based on Carbonized Bamboo Fibers for Wide Temperature Applications. *Sci. Rep.* **2016**, *6* (August), 31704.

(31) Gomez, J.; Kalu, E. E. High-Performance Binder-Free Co–Mn Composite Oxide Supercapacitor Electrode. *J. Power Sources* **2013**, *230*, 218–224.

(32) Mujawar, S. H.; Ambade, S. B.; Battumur, T.; Ambade, R. B.; Lee, S.-H. Electropolymerization of Polyaniline on Titanium Oxide Nanotubes for Supercapacitor Application. *Electrochim. Acta* **2011**, *56* (12), 4462–4466.

(33) Mitchell, E.; De Souza, F.; Gupta, R. K.; Kahol, P. K.; Kumar, D.; Dong, L.; Gupta, B. K. Probing on the Hydrothermally Synthesized Iron Oxide Nanoparticles for Ultra-Capacitor Applications. *Powder Technol.* **2015**, *272*, 295–299.

(34) Mitchell, E.; Jimenez, A.; Gupta, R. K.; Gupta, B. K.; Ramasamy, K.; Shahabuddin, M.; Mishra, S. R.; Kumar, N. A.; Baek, J.-B.; Wu, Z.-S.; et al. Ultrathin Porous Hierarchically Textured $NiCo_2O_4$–graphene Oxide Flexible Nanosheets for High-Performance Supercapacitors. *New J. Chem.* **2015**, *39* (3), 2181–2187.